Journal of Structural Geology 124 (2019) 120–135

Contents lists available at ScienceDirect

Journal of Structural Geology

journal homepage: www.elsevier.com/locate/jsg

Structure, emplacement mechanism and magma-flow significance of igneous fingers – Implications for sill emplacement in sedimentary basins

Olivier Galland[a,*], Juan B. Spacapan[b,c], Ole Rabbel[a], Karen Mair[a], Frederico González Soto[d], Trond Eiken[e], Mario Schiuma[f], Héctor A. Leanza[g]

[a] Physics of Geological Processes, The NJORD Centre, Department of Geosciences, University of Oslo, Box 1047, Blindern, 0316, Oslo, Norway
[b] Universidad Nacional de la Plata-CONICET-Fundación YPF, 1900, La Plata, Argentina
[c] Now at Y-TEC, Av. del Petróleo Argentino, 900-1198, Berisso, Buenos, Aires, Argentina
[d] Universidad Nacional de La Plata – ANPCyT IGS CISAUA, 1900, La Plata, Argentina
[e] Department of Geosciences, University of Oslo, Box 1047, Blindern, 0316, Oslo, Norway
[f] YPF, Buenos Aires, Argentina
[g] Museo Argentino de Ciencias Naturales-CONICET, 1405 Buenos Aires, Argentina

ARTICLE INFO

Keywords:
Igneous fingers
Viscoelastic fingering
Viscous indenter
Magma-flow indicators
Integrated drone survey/field measurements

ABSTRACT

Field and seismic observations show that numerous sills exhibit lobate morphologies. Each lobe corresponds to a distinct igneous segment exhibiting a finger-like shape, the long axis of which is commonly interpreted as a magma-flow indicator. Robust understanding of the emplacement mechanisms of finger-shaped sills, and direct observations supporting finger orientation as magma-flow indicator are lacking. In this paper, we present the results of detailed structural mapping on an exceptional, easily accessible 1-km long outcrop in the Neuquén Basin, Argentina, that exhibits a sill, its contacts and the structures in the finely layered sedimentary host rock. We show that the sill is made of distinct segments that grew, inflated or coalesced. We also demonstrate that the fingers were emplaced according to the viscoelastic fingering or viscous indenter models, with no field evidence of tensile elastic fracture mechanism as commonly assumed in mechanical models of sill emplacement. We identified new structural criteria at the intrusion's contacts for inferring magma flow direction during the magma emplacement. Our small-scale structural observations carried out on a seismic-scale outcrop have the potential to considerably aid the structural interpretation of seismic data imaging igneous sills, i.e. to fill the standard gap between outcrop-scale field observations and seismic-scale geophysical data.

1. Introduction

Igneous sheet and tabular intrusions, such as dykes, sills and laccoliths, are fundamental magma conduits and reservoirs through the Earth's crust (e.g., Walker, 1975; Rubin, 1995; Petford et al., 2000; Cartwright and Hansen, 2006; Magee et al., 2016). In particular, the last two decades of research have highlighted that voluminous sill complexes accommodate extensive lateral and vertical magma transport and emplacement in sedimentary basins worldwide (Magee et al., 2016; Galland et al., 2018), such as offshore Norway (e.g., Svensen et al., 2004; Planke et al., 2005), the Karoo Basin, South Africa (Chevallier and Woodford, 1999; Polteau et al., 2008; Galerne et al., 2011), the Rockall Basin, offshore Ireland (Thomson, 2004; Thomson and Hutton, 2004; Hansen and Cartwright, 2006b; Magee et al., 2014), the Faeroe-Shetland Basin (Trude et al., 2003), Greenland (Eide et al., 2016), the Neuquén Basin, Argentina (Rodriguez Monreal et al., 2009; Witte et al., 2012; Rabbel et al., 2018; Spacapan et al., 2018), offshore Australia (Symonds et al., 1998; Jackson et al., 2013; Magee et al., 2013) and Antarctica (Jerram et al., 2010; Muirhead et al. 2012, 2014).

Most mechanical models of sill emplacement consider sills and laccoliths as continuous igneous sheets, emplacing and propagating as hydraulic fractures (Pollard, 1973; Kavanagh et al., 2006; Bunger and Cruden, 2011; Michaut, 2011; Galland and Scheibert, 2013). These models assume that the host rock behaves as a purely elastic medium, and that there is a single peripheral propagating edge. However, in many basins, igneous sills are preferentially emplaced into formations of certain lithologies, often shale (e.g., Rossello et al., 2002; Thomson, 2007; Rodriguez Monreal et al., 2009; Schofield et al., 2012a; Witte et al., 2012; Magee et al., 2014; Spacapan et al., 2018), which can deform in an inelastic manner (Fig. 1; Pollard et al., 1975; Schofield

* Corresponding author.
E-mail address: olivier.galland@geo.uio.no (O. Galland).

https://doi.org/10.1016/j.jsg.2019.04.013
Received 3 November 2018; Received in revised form 17 April 2019; Accepted 19 April 2019
Available online 21 April 2019

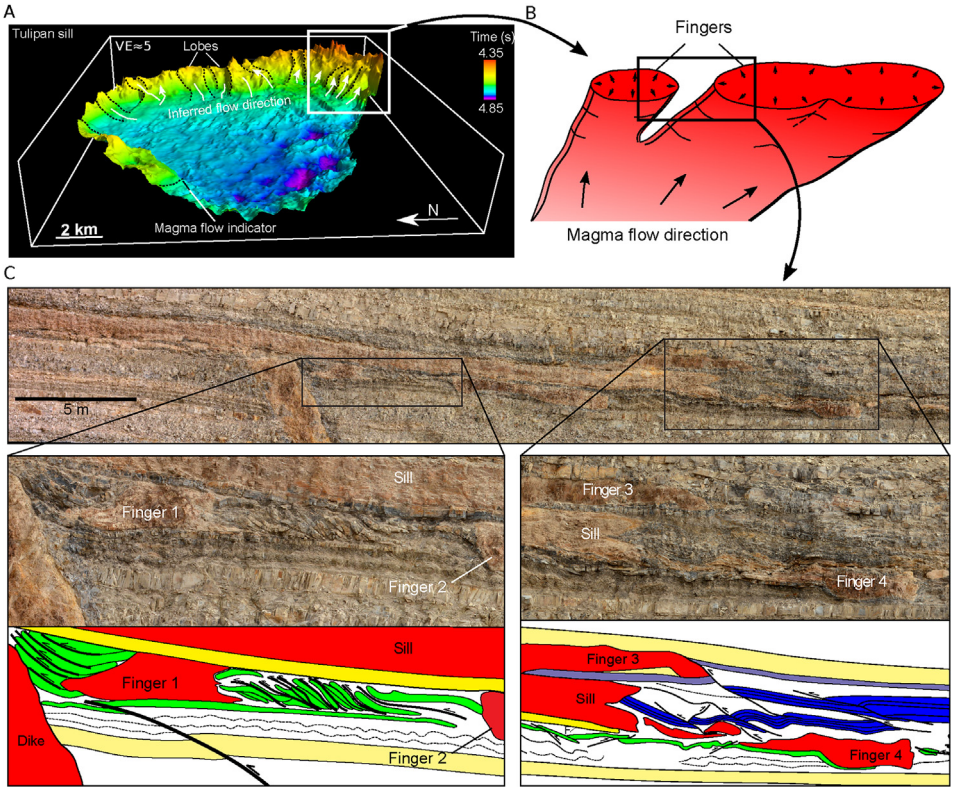

Fig. 1. A. 3D seismic cube of the Tulipan saucer-shaped sill, Møre Basin, offshore Norway (Schmiedel et al., 2017b). Lobes along inclined sheets are interpreted as fingers and outward flow directions. B. Schematic drawing of the morphology of igneous fingers and their interpreted magma-flow directions (Galland et al., 2018, and references therein). C. Top: outcrop photograph of andesitic fingers emplaced in layered shale-dominated sedimentary rocks, Cuesta del Chihuido, southern Mendoza Province, Argentina (Spacapan et al., 2017). Lower: zoomed field photographs and interpreted drawings of igneous fingers and surrounding structures in the host rock. All structures indicate shortening accommodating edge propagation of the fingers.

et al., 2012a; Wilson et al., 2016; Spacapan et al., 2017). This strongly questions the applicability of the purely elastic models to address the emplacement of sills in weak rock formations, particularly in shale (Scheibert et al., 2017).

Field observations (Pollard et al., 1975; Schofield et al., 2012a; Spacapan et al., 2017) and 3D seismic data (Hansen and Cartwright, 2006a; Thomson, 2007; Schofield et al., 2012a; Magee et al., 2016; Schmiedel et al., 2017b) show that numerous sills emplaced in weak rock formations exhibit lobate morphologies (Fig. 1), each lobe corresponding to a distinct igneous segment and exhibiting finger-like shapes. The fingers can subsequently coalesce to form a continuous, stepped sheet with broken bridges or simple intrusive steps between the segments (Magee et al., 2018). These observations suggest that the propagation of igneous sills does not occur along a peripheral, simple front, but through the propagation of multiple lobate fronts that can eventually coalesce. In addition, the long axes of igneous fingers are commonly interpreted as magma flow indicators (e.g., Magee et al., 2018) (Fig. 1). However, in outcrop, the shape of a finger is insufficient to determine in which direction the magma was flowing through, except if the overall intrusion is exposed (Polteau et al., 2008).

Revealing the emplacement mechanism of igneous fingers is essential for (1) understanding the dynamics of sill and laccolith emplacement in weak rock formations and (2) retrieving magma flow directions through the fingers. These mechanisms are not yet well understood. Pollard et al. (1975) suggested that the growth of igneous fingers into their host rock is governed by a Saffman-Taylor instability (Saffman and Taylor, 1958), i.e. the interface between an intruding magma and a viscous host rock is mechanically unstable and grows by developing digitations, or fingers. Such a mechanism is very close to the viscoelastic fingering mechanism, where the intruding viscous magma indents the host rock, as highlighted by laboratory experiments (e.g., Mathieu et al., 2008; Nase et al., 2008; Bertelsen et al., 2018; Poppe et al., 2019). Such mechanism is also close to the viscous indenter model, as inferred by Spacapan et al. (2017), which states that fingers grow by pushing the host rock, which fails by brittle or ductile faulting (see also Pollard, 1973; Donnadieu and Merle, 1998; Merle and Donnadieu, 2000). Finally, Schofield et al. (2010; 2012a) and Jackson et al. (2013) suggest that the propagation of magma is accommodated by fluidization of the host rock.

Studying the detailed mechanisms of igneous finger emplacement remains challenging. First, the resolution of seismic data is insufficient to document the small-scale structures that accommodate the propagation of igneous fingers and magma flow indicators (e.g., Magee et al., 2016; Eide et al., 2017; Rabbel et al., 2018). Second, the detailed structures accommodating the emplacement and growth of igneous fingers are rarely well exposed and/or preserved (Pollard et al., 1975; Horsman et al., 2005; Schofield et al., 2012a; Spacapan et al., 2017). In this paper, we present the results of detailed structural mapping of an exceptional, easily accessible 1-km long outcrop at Las Loicas, located in the Neuquén Basin, Argentina (Fig. 2), which exhibits a sill composed of a string of igneous fingers, their contacts and the structures in their finely layered sedimentary host rock. This outcrop (1) reveals how the host rock accommodates the emplacement of the fingers, and (2) provides direct structural evidence of magma flow direction through the studied fingers.

2. Geological setting: the Neuquén Basin, Argentina

The studied outcrop is situated along the Río Grande Valley, located in southern Mendoza province, Argentina, between 36° S and 36.5° S (Fig. 2). It is located 6 km east of the village of Las Loicas, along the national road RN145 that crosses the Andes to Chile. The outcrop is part of the Malargüe fold-and-thrust belt in the main Andes, in the northern sector of the Neuquén Basin; it is located in the northern prolongation of a basement-cored anticline, the Sierra Azul Anticline.

The evolution of the basin took place in three stages or phases (Howell et al., 2005; Vergani et al., 1995; Horton et al., 2016): (1) rift stage or synrift phase (Late Triassic – early Early Jurassic), (2) thermal subsidence (sag) stage or postrift phase (late Early Jurassic - Early Cretaceous), and (3) foreland stage (Late Cretaceous-Neogene), related to Andean uplift. The host rock formations of the studied sills are sedimentary rocks deposited during the thermal subsidence stage and

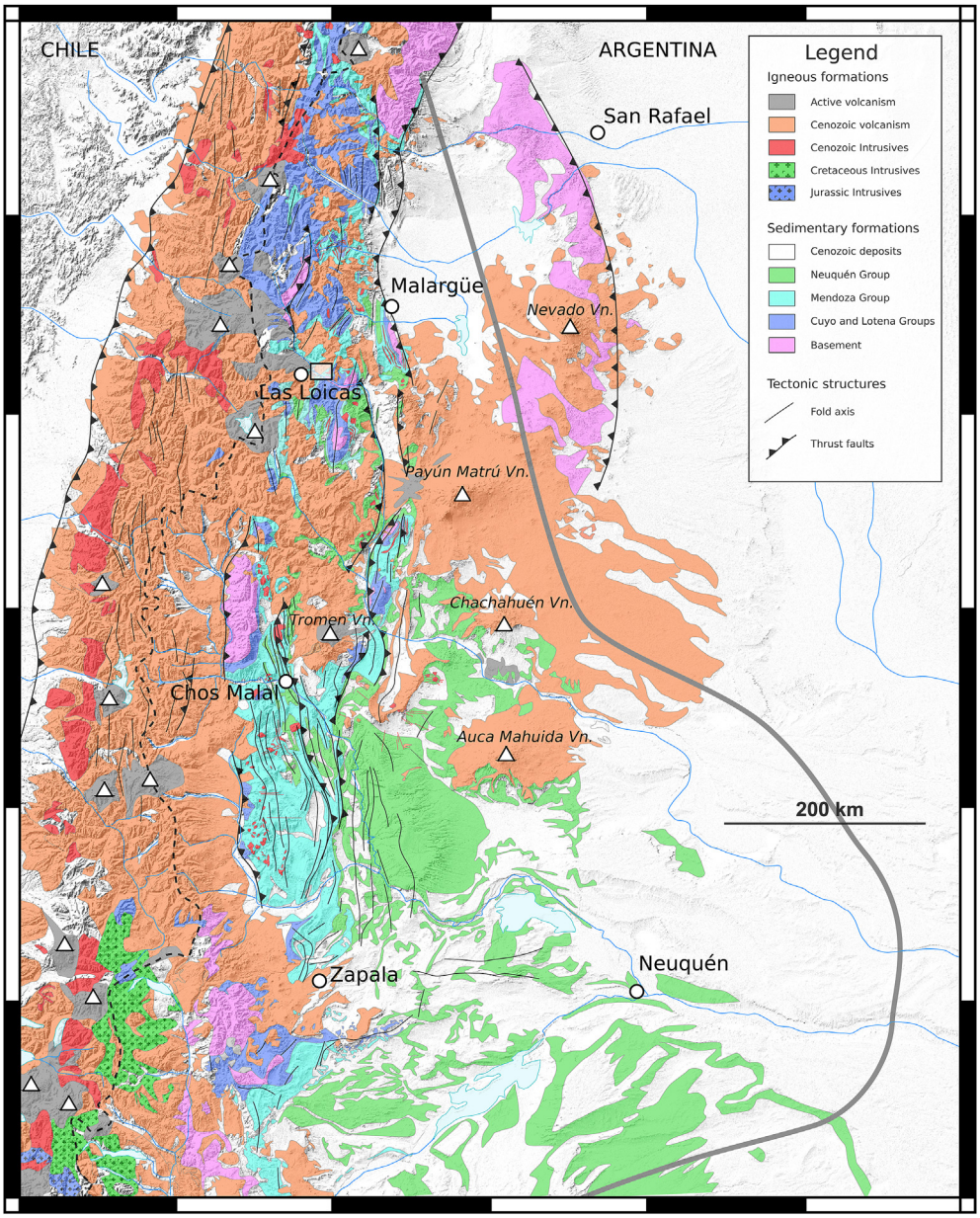

Fig. 2. Simplified geological map of the Neuquén Basin and surroundings. The map compiles geological maps of Chile (Sernageomin, 2003), of Neuquén Province (Delpino and Deza, 1995) and of Mendoza Province (Caminos et al., 1993). White triangles indicate both arc and back-arc Upper Miocene-Holocene volcanoes. Grey line locates boundary of Neuquén Basin. Study area is located just east of Las Loicas village (transparent white rectangle).

belong to the Mendoza Group, which consists of: (1) the Tithonian - Early Valanginian Vaca Muerta Formation (ca. 125–140 m thick), composed of bituminous shales, deposited under anoxic conditions of shelf and slope marine settings, (2) the Middle Valanginian Chachao Formation (ca. 35–50 m thick), deposited above the Vaca Muerta Formation, consisting of a carbonate ramp full of biogenic material (Kozlowski et al., 1993; Brissón and Veiga, 1998), and (3) the Late Valanginian – Early Barremian Agrio Formation (ca. 250–300 m thick) deposited as a transgressive organic-rich marly shale.

In the Early Cretaceous, the retroarc-subsidence phase ended and the tectonic regime transitionally changed to compressive, due to a decrease in the subduction angle of the Nazca plate and the beginning of the Andean orogeny (Cobbold and Rossello, 2003; Ramos et al., 2010). During this time, inversion of the normal faults of the Triassic rifts and reactivation of older basement faults led to the formation of the Malargüe Fold-and-Thrust Belt (e.g., Giambiagi et al., 2005; Horton et al., 2016; Fennell et al., 2017). The uplift of these structures could have begun in the Late Cretaceous (Tunik et al., 2010; Folguera et al., 2015; Fennell et al., 2017) and continued during the Paleogene to the Neogene (Silvestro and Kraemer, 2005; Orts et al., 2012; Álvarez Cerimedo et al., 2013).

The Miocene was characterized by two significant volcanic cycles: the Late Oligocene - Middle Miocene Molle Eruptive Cycle (MEC) and the Late Miocene-Pliocene Huincán Eruptive Cycle (HEC) (Combina and Nullo, 2011). These eruptive cycles resulted in thick lava flow sequences, such as the Puntilla del Huincán lavas (Combina and Nullo, 2011) and the Payunia volcanic field (e.g., Dyhr et al., 2013; Søager et al., 2013). In addition, these eruptive cycles resulted in numerous andesitic to basaltic sills (Rabbel et al., 2018), which likely formed parts of the plumbing system. The main intrusions range from 23.6 Ma to 2.7 Ma in age (Silvestro and Atencio, 2009) and are dominantly emplaced in the source rock formations of the Mendoza Group (Schiuma, 1994b; Monreal et al., 2009; Spacapan et al. 2018, 2019).

The outcrop described in this study consists of series of exposed

andesitic fingers and a sill, aligned sub-parallel to the layering of the host rock. Although the fingers and sill appear disconnected in outcrop, they are likely connected in the third dimension as one large andesitic sheet, as they exhibit very similar andesitic composition and magmatic texture. They are emplaced in the organic-rich shales of the Mendoza Group, but whether the host rock is the Vaca Muerta Fm. or the Agrio Fm. is unknown. The lateral extent of the sill is unknown as it is affected to the south by tectonic structures of the Malargüe fold-and-thrust belt and it is partly covered by Cenozoic volcanic deposits. The emplacement depth of the studied intrusive is challenging to constrain, given the amount of tectonic shortening and denudation of the overburden. In the study area, the emplacement depth of sill complexes in the shale of the Mendoza groups is estimated between 2000 and 2500 m depth (Witte et al., 2012; Rabbel et al., 2018; Spacapan et al., 2018).

3. Field observations

This section describes successively (1) the morphology of the units of the intrusive complex, (2) the structures in the host rock that accommodated the emplacement of the magma, and (3) the structures observed at the contact between the intrusions and the host rock.

3.1. Main intrusive units

From NW to SE, we define the following units: a Main Sill, two fingers having relatively simple shapes in the exposed section (Finger1 and Finger2), and a unit of more complex shape, Finger3, that marks the end of the intrusive complex (Fig. 3 and Fig. 4).

The Main Sill is a continuous sheet-like intrusive unit that extends several kilometres to the NW and W, until at least the Las Loicas Village. It has a relatively constant thickness of ~30 m. Its upper and lower contacts are overall concordant with the layering of the host rock, which dip ~35° to the SW (Figs. 3 and 4B). Nevertheless, it exhibits sharp, 5–10 m high steps at both the upper and lower contacts (Fig. 5), where they are locally discordant to the host's layering. The edge of the Main Sill is exposed close to Finger1; it has a rounded shape, and the contact with the host rock becomes vertical and highly discordant.

Finger1 is the thickest unit of the outcrop (up to ~50 m; Fig. 5) with thickness-to-width aspect ratio ~1/3. Upper and lower contacts are overall concordant (Figs. 4 and 5A), but local undulations crosscut the host rock layers (e.g. Fig. 4D). Its NW edge is rounded with wavy irregularities, whereas its SE edge is almost rectangular and in part vertical, in contact with Finger2 (Fig. 5).

Finger2 exhibits a similar shape to that of Finger1, with an aspect ratio even lower (< 1/2). Its NW edge is also almost squared with a vertical contact touching Finger1. Its SE edge has an overall vertical contact, but it exhibits several cylindrical bulges (Figs. 5 and 6A). It is separated from Finger3 by a thin sliver of sedimentary host rock (Figs. 5 and 6A).

Finger3 exhibits a more complex and irregular shape than other intrusive units (Figs. 3 and 5). Its lower contact is relatively regular and concordant with the host layering, whereas the upper contact is very wavy with many local discordant contacts, leading to varied finger thickness from ~5 m to ~20 m (Fig. 5). The NW edge is rounded and exhibits lobate morphology (Figs. 5 and 6A), whereas the SE edge thins before terminating (Fig. 5).

The andesite exhibits clear fracture patterns that resemble columnar jointing related to magma cooling. In the Main Sill, most joints are subvertical, except at the SE edge where the joints are radial, perpendicular to the rounded intrusion's contact (Fig. 6B). In Finger1, the dominant joint fabric is vertical, except along the contacts at the NW edge and upper corner of the SE edge, where joints are radial and subperpendicular to the Finger's contact. Similar features are visible all around Finger2 and at the NW edge of Finger3 (Fig. 6). In the main part of Finger3, the joint fabric is more chaotic (Fig. 5).

The andesite of Finger3 is cut by two faults (Figs. 5 and 7) dipping to the west and to the northwest (Fig. 7). Kinematic indicators on the west-dipping fault point to a reverse fault.

3.2. Structures at intrusions' contacts

We systematically mapped the structure of the intrusions' contacts along the studied outcrop (Fig. 8). All structural measurements are displayed in Fig. 9, and include strike/dip measurements and kinematic indicators on the intrusive contacts (Fig. 8, stereograms of Fig. 9), and strike/dip measurements of, and structures deforming, host rock layers (symbols on map of Fig. 9). Note that no measurements were performed on the upper contacts of Finger1 and Finger2, since accessing these contacts without safety mountaineering equipment was deemed hazardous (see for example field photograph of Fig. 4A).

Measurements of the intrusive contacts provide constraints on the shapes of the intrusive units and their relationship with the layering of the host rock. Most upper and lower contacts of the Main Sill, Finger1 and Finger2 dip towards the SW at ~30° on average (Fig. 9) consistent with the average layering of the host rock. A similar trend is observed for the lower and upper contacts of Finger3, but more scattering of the measurements reflects the irregular shape of this unit (Fig. 5). We note that the measured contacts of the edges of all intrusive units are subvertical and strike between N40 and N50. Interpolating between the upper, lower and edge contacts, the exposed parts of Finger1 and Finger2 are approximated as slices of tubes, having the axes parallel to the overall dip direction of the host rock's layering, i.e. sub-perpendicular to the outcrop. The Main Sill has the shape of a flat ellipse, with a long axis parallel to the dip direction of the host rock's layering. Note

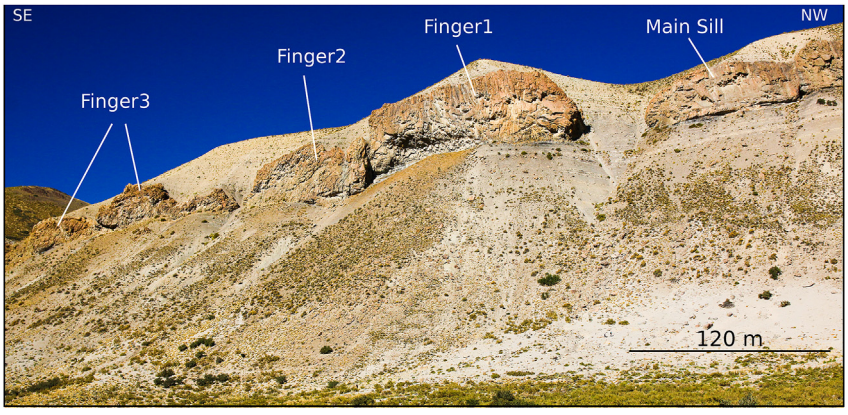

Fig. 3. Field photograph of entire studied outcrop. It stretches south of National Road 145, 6 km east of Las Loicas village. Andesitic intrusions are emplaced in organic-rich shale of the Mendoza Gr.

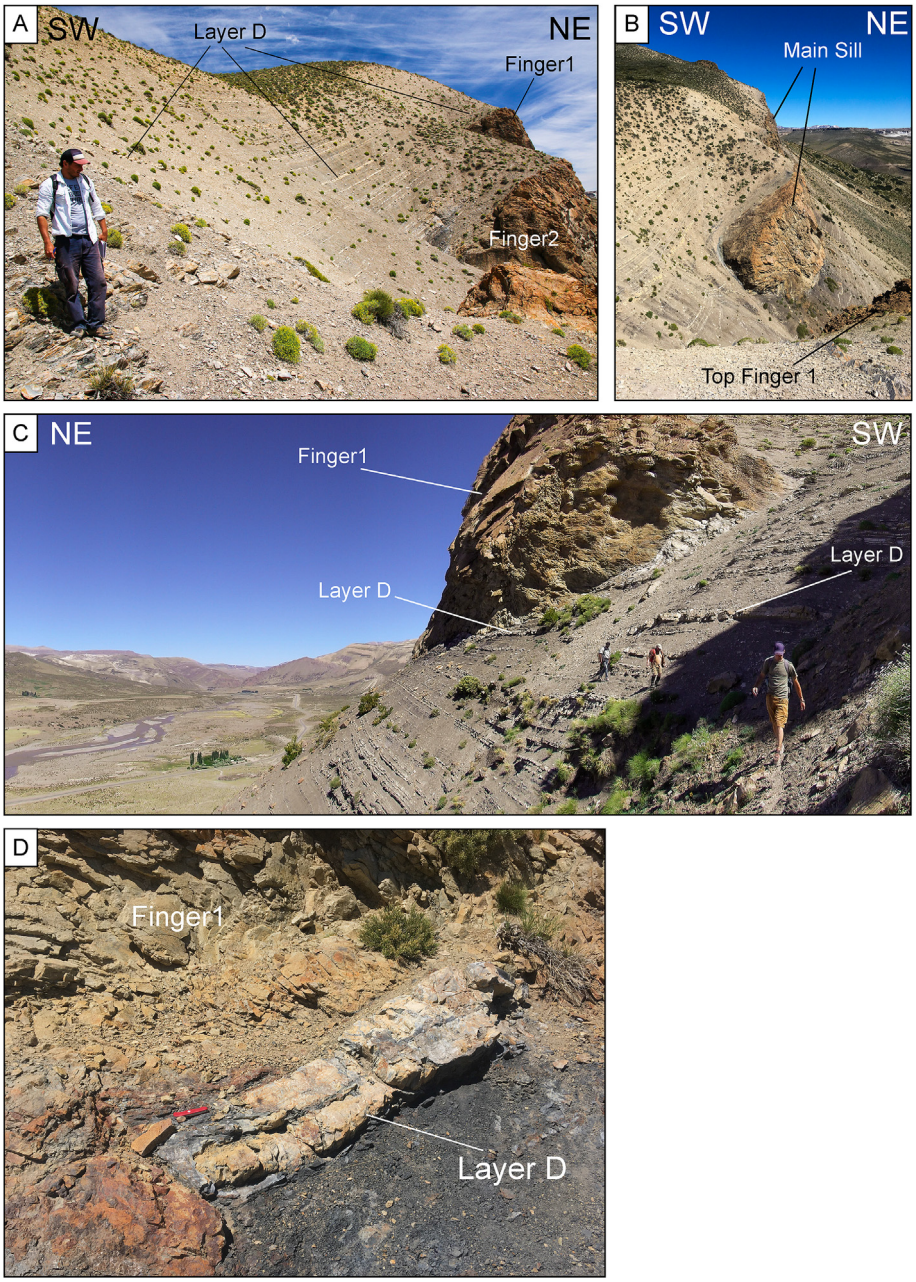

Fig. 4. Field photographs of main units of the studied outcrop. A. Westward view above Finger2 and Finger1. B. Westward view above Main Sill, from above Finger1. C. Eastward view of bottom of western edge of Finger1, viewed from below edge of Main Sill. D. Close up photograph of marker Layer D.

that the vertical planes of stereogram "Edge Finger3" strike N70-N85, i.e. slightly distinct from the main N40 and N50 trends of the inferred fingers' axes and likely correspond to the extreme edge of the intrusive complex.

Many upper and lower intrusive contacts exhibit striations (Figs. 8 and 9). Most of these contacts are concordant with the local host rock's layering. On the upper contacts of Finger3, kinematic indicators provided by striations' asperities indicate top-to-the-SW movements, whereas on the lower contacts of Finger3, the kinematic indicators indicate opposite top-to-the-NE movements (Fig. 9).

Top-to-the-NE movements were also measured at the lower contact of Finger2 (Fig. 9). On the contact of the SE edge of Finger2, kinematic indicators provide dextral movement along sub-vertical planes striking N70-N80 (Fig. 9). The slickenside on the upper contact of Finger2, close to the SE edge, indicates top-to-the-west movement (Fig. 9).

Finally, the only kinematic indicators along the contacts of the Main Sill were observed at the upper contact, close to its edge. Slickensides' asperities indicate top-to-the-west movement.

The vertical intrusive contacts at the edge of the Main Sill and at the SE edge of Finger2 exhibit meter-scale and decimetre-scale undulations (Figs. 8B and 9). The undulations' axes consistently plunge ~30° on average toward the SW.

3.3. Structures in the host rock

The outcrop has characteristics useful for studying emplacement processes of igneous fingers: (1) the distinct lithologies of the intrusive units and of the sedimentary host rocks make the mapping of the intrusive contacts straightforward, and (2) the host rock is thinly layered, so that detailed structural mapping allows one to infer the kinematics of how intrusive emplacement was accommodated. We performed a detailed structural mapping of the host rock's layers, similar to that of

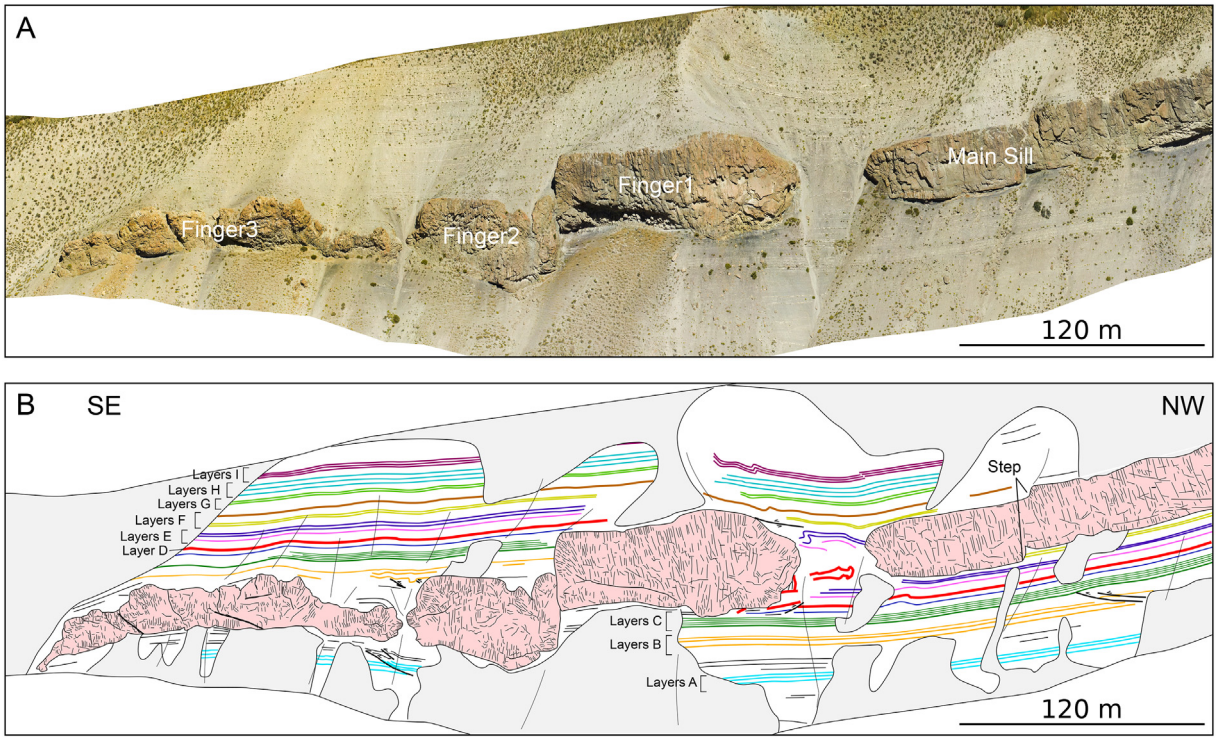

Fig. 5. A. Orthorectified image of studied outcrop computed using 126 drone photographs. B. Structural interpretation of orthorectified image. Faults are indicated as bold black lines. Note marker Layer D shown in red. (For interpretation of the references to colour in this figure legend, the reader is referred to the Web version of this article.)

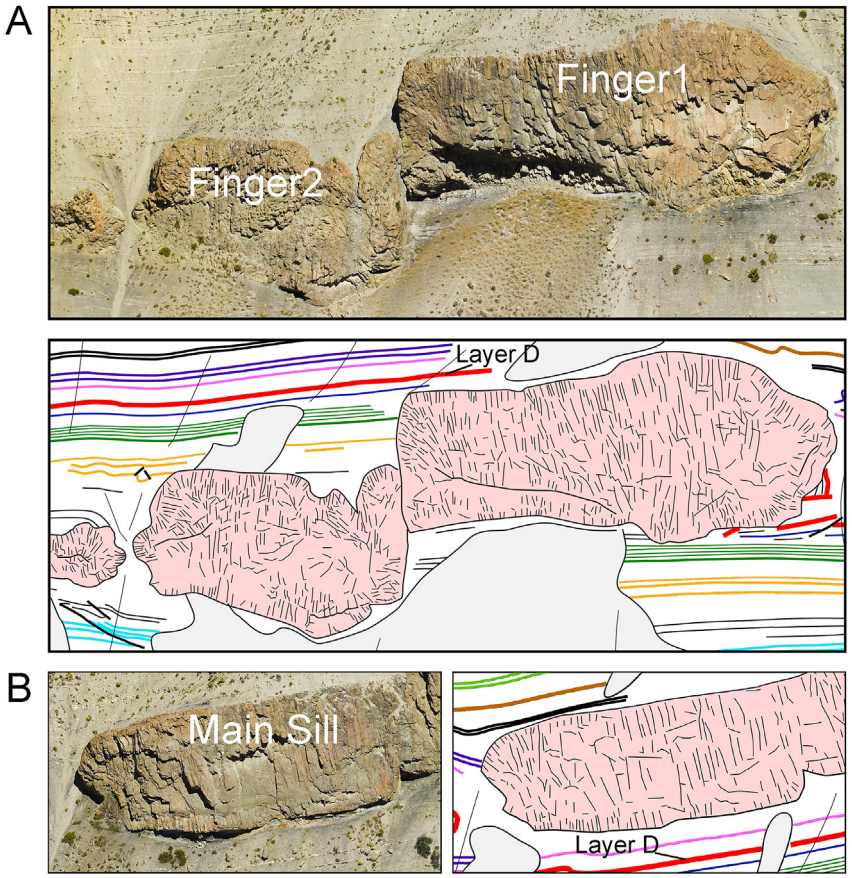

Fig. 6. A. Detailled orthorectified image of Finger1 and Finger2 (top) and interpreted structural drawing (bottom). Note radial fractures close to fingers' walls. B. Detailled orthorectified image of edge of Main Sill (left) and interpreted structural drawing (right). Note as well radial fractures at sill's edge.

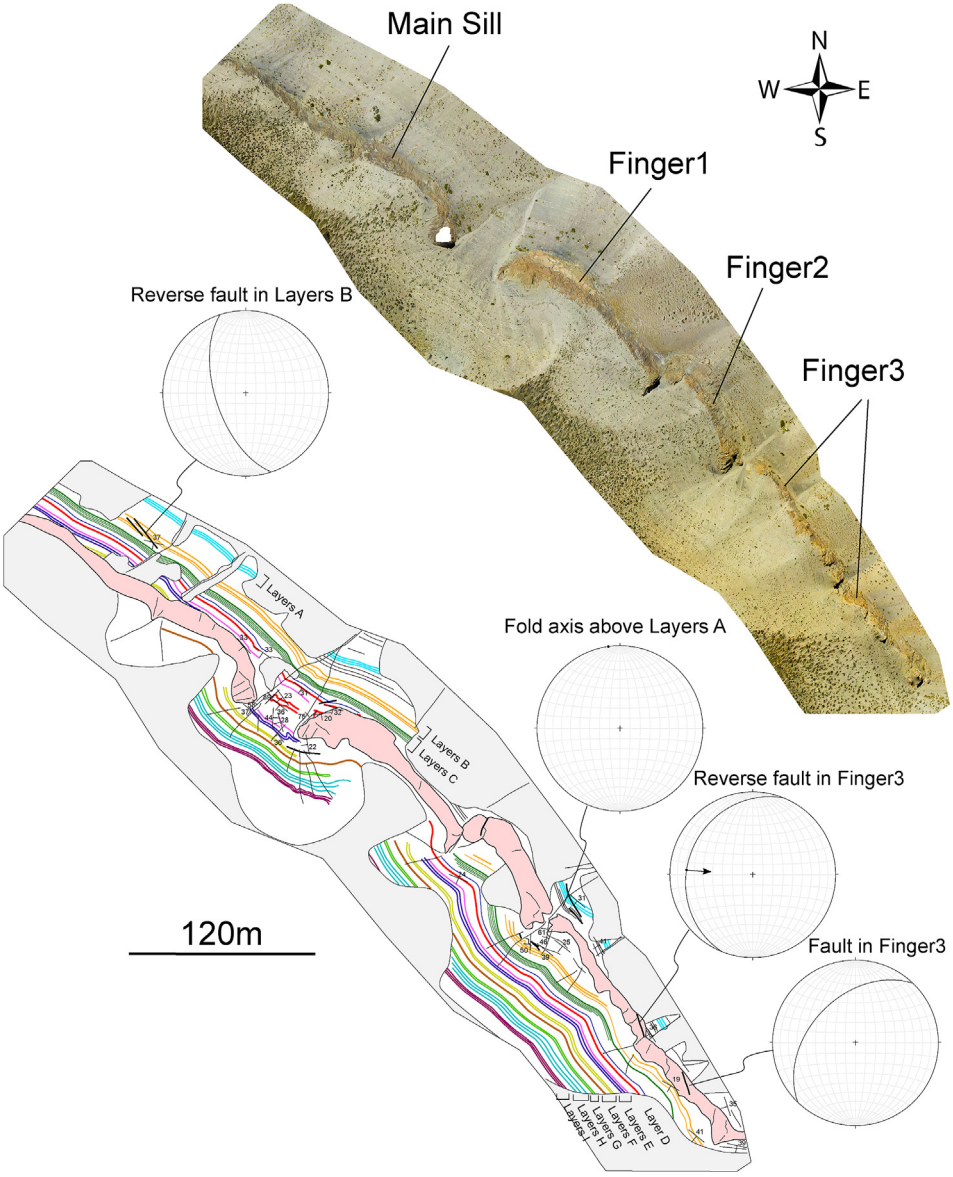

Fig. 7. A. Bird's eye (vertical) view orthorectified image of studied outcrop with location of intrusive units and interpreted layers of Fig. 6. B. Interpretative geological map of orthorectified image and lower hemisphere stereograms of interpreted tectonic structures.

Spacapan et al. (2017).

The host rock consists of a succession of fine-grained carbonate layers within shale. We identified one key marker layer, the so-called Layer D, which consists of a double carbonate bed separated by a few-cm thick shale-rich layer (Fig. 4D). This layer is continuously present above Finger2, Finger3, and the SE edge of Finger1, and also below the Main Sill and the NW edge of Finger1 (Figs. 4, Figs. 5 and 7). Thanks to this marker, all the other layers can be correlated confidently throughout the outcrop, with the exception of the layers outcropping below Finger3 (Fig. 5). We named the identified layers from the lowermost Layers A to the uppermost Layers I. In the following paragraphs, we describe the host rock's structures by sectors, from large-scale patterns to details.

Above Finger3, Finger2 and the SE edge of Finger1, Layers B to Layers I exhibit regular dip to the SW by ~40° on average (Figs. 5 and 7). The same regular dipping is observed for (1) Layers F to Layers I above the Main Sill and the gap between the Main Sill and Finger1, (2) Layers A to Layers C below the Main Sill and the NW edge of Finger1 (Figs. 5 and 7). Discontinuous outcrop condition below Finger1 to below Finger3 makes structural interpretation tentative. We also observed a prominent fold structure above Finger1 (Fig. 5), but the locally steeper slope of the terrain makes access and measurement hazardous, and the structure is partly covered by slope deposits.

We observed numerous structures deforming the host rock's layers between the Main Sill and Finger1. Layer D is duplicated, and intensely folded (Fig. 10). Sharp variations in dip of the layers record strong folding of all the layers and numerous small faults truncate the layers (Fig. 10). All the observed structures indicate intense shortening of the layers. The main fold axes, systematically trending NE-SW, indicate local NW-SE shortening, i.e. perpendicular to the subvertical intrusive contacts at the edges of the Main Sill and of Finger1. Note that this shortening is present only between the edges of the Main Sill and of Finger1, but is absent in the underlying Layers A to Layers C and in the overlying Layers G to Layers I above (Fig. 10), indicating detachments between the folded layers and the non-deformed layers.

We also observed folds and some faults accommodating shortening of the Layers B above the NW edge of Finger3 (Fig. 11). The fold axes, tending NE-SW, indicate NW-SE shortening perpendicular to the subvertical intrusive contact of the SE edge of Finger2. Shortening affects only the Layers B, but not the layers above, indicating a local

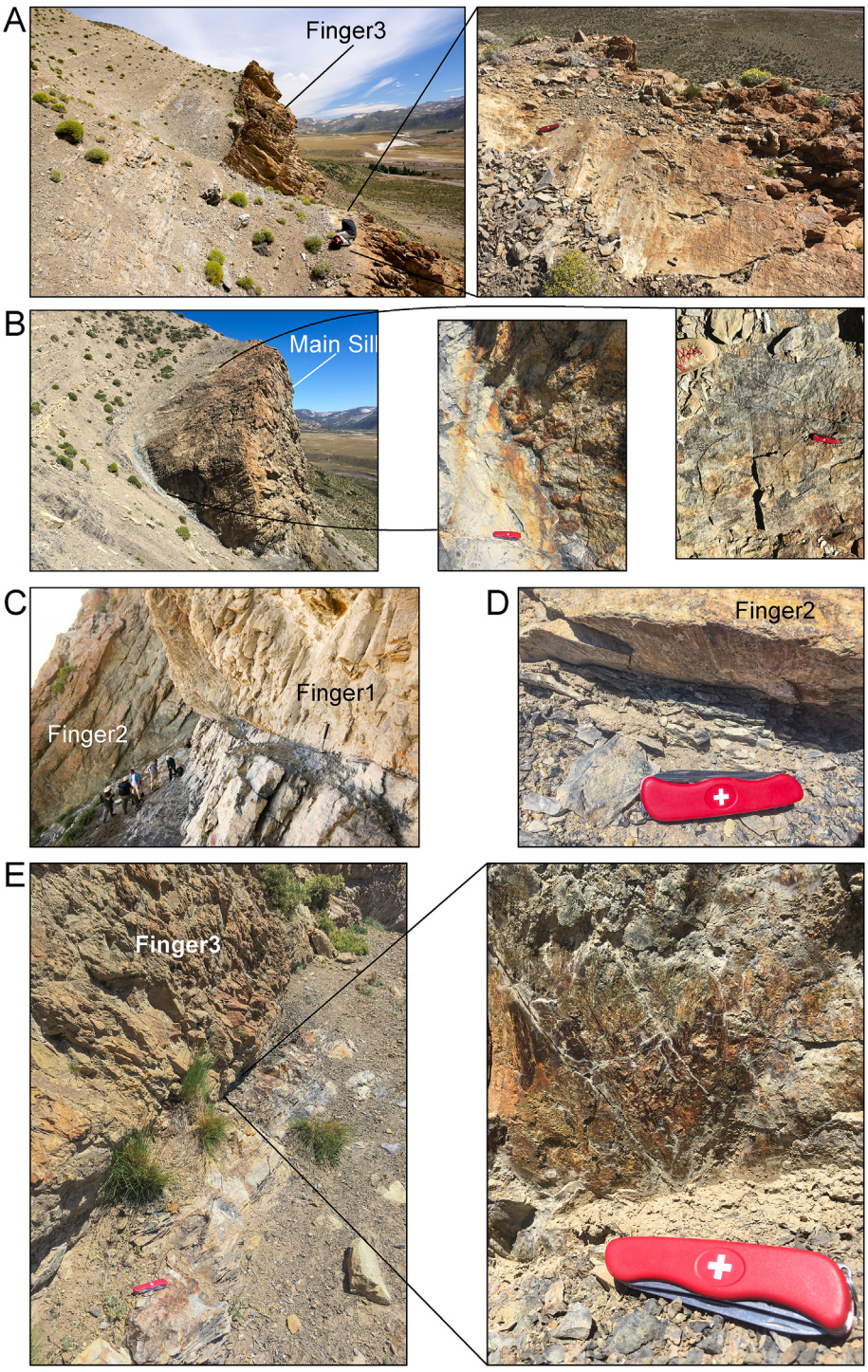

Fig. 8. Characteristic field photographs of contacts of main intrusive units. A. Large field photograph (left) locating close up of upper contact (right) of Finger3. Note slickensides on contact plane. B. Large field photograph (left) of edge of Main Sill. Close up of contact at edge (center) showing undulating lineation of contact (see location on left image). Close up of top contact (right) showing well-developed slickensides on contact. C. Bottom contact of Finger1, near Finger2. D. Close up photograph of bottom contact of Finger2 with slickensides on contact plane. E. Large field photograph (left) and close up (right) of bottom contact of Finger3; note as well slickensides on contact plane.

detachment (Figs. 5 and 11).

We observed other minor structures in the host rock that are not adjacent to the intrusions' edges. Below the Main Sill, a series of small-offset west-dipping reverse faults affect Layers B (Figs. 5 and 7). Below the NW edge of Finger3 and the SE edge of Finger2, Layers A are folded and faulted (Figs. 5 and 7); the observed fold axis trends almost N-S (Fig. 7).

4. Interpretation

4.1. Intrusion shapes are primary structures

The study area is located in a fold-and-thrust belt, meaning it is necessary to assess whether the observed structures are related to the emplacement of the intrusions or of tectonic origin. The contact between Finger1 and Finger2 and the step observed in the Main Sill could be interpreted as sub-vertical tectonic faults. Our detailed observations, however, lead to another interpretation.

First, our observations show that the fracture patterns in the intrusive units, close to their contact, are systematically sub-

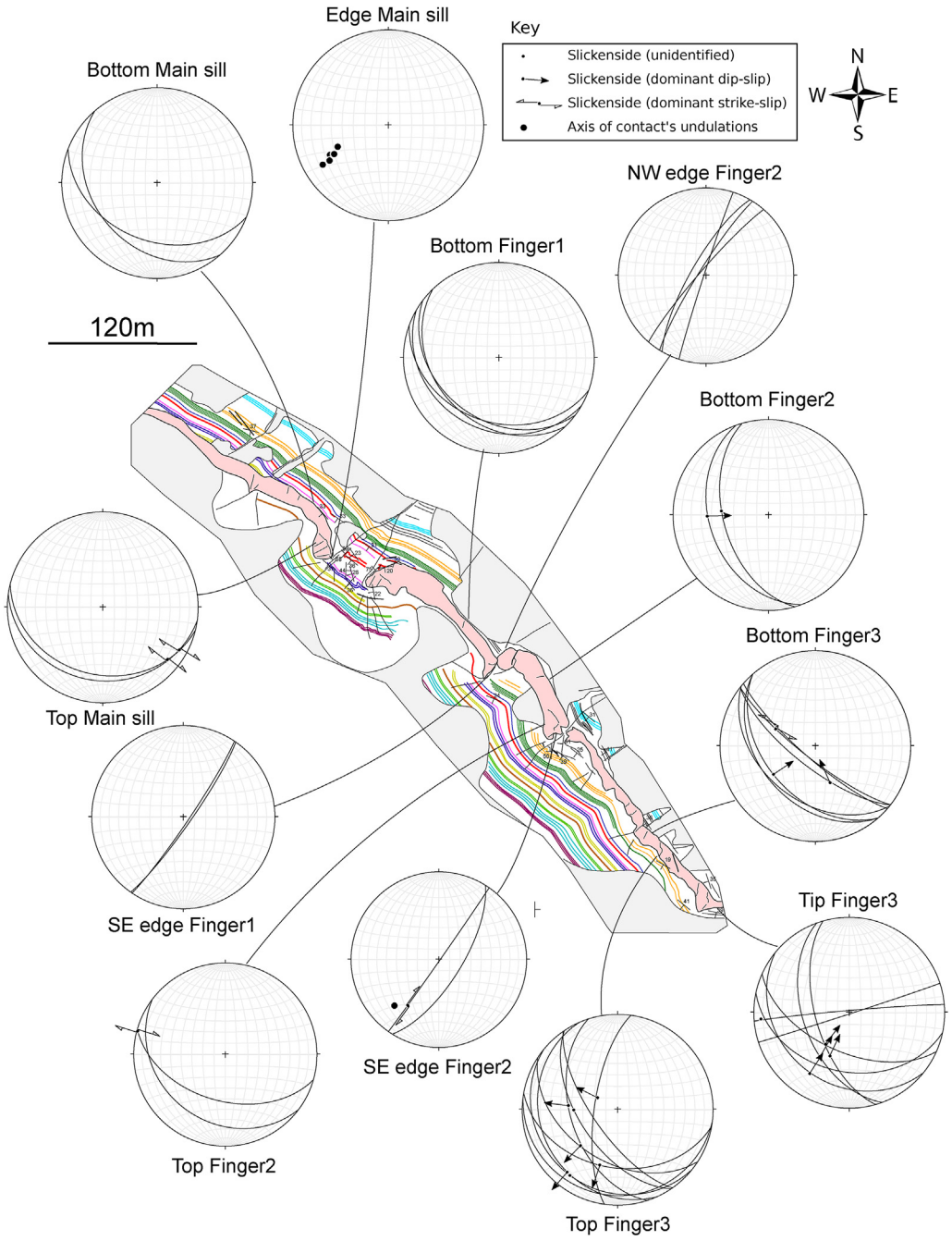

Fig. 9. Lower hemisphere stereograms of field measurements of intrusions' contacts along studied outcrop, located on interpretative geological map of Fig. 7B.

perpendicular to intrusions' contacts (Fig. 6). Such fracture patterns are typical of cooling joints, meaning that the intrusive units cooled in their current shapes.

Second, the structures that disturb the host rock's layers are dominantly confined in between the intrusive units, and are absent above and below the intrusive units (Figs. 10 and 11). In addition, Layers A to Layers E below the step in the Main Sill are straight and not offset, even very close to the step. Finally, the apparent offset between Finger1 and Finger2 would indicate that Finger1 moved upward with respect to Finger2, which is in contradiction with the apparent offset of Layers C that shows the opposite movement. Hence, if these structures were of tectonic origins, they would affect the whole layer sequence. We therefore infer that they are related to the emplacement of the intrusive units.

Nevertheless, we cannot rule out that some structures are related to tectonic deformation, such as the minor faults below the Main Sill and the fold above Finger1. In addition, faults observed within Finger3 indicate that it was affected by some post-emplacement tectonic deformation. Nevertheless, these minor faults did not significantly offset the intrusion, showing that they are of secondary importance with respect to the emplacement-related structures.

4.2. Intrusion shape and magma flow direction indicators

The studied outcrop provides a dominant 2D exposure of the igneous fingers described in this study. However, the intrusion contacts in the third dimension, i.e. perpendicular to the outcrop, are also well exposed. Given the systematic NW strike and SW dip direction directions of the upper and the lower contacts, as well as the systematic NW strike of the sub-vertical contacts at the intrusions' edges, we naturally

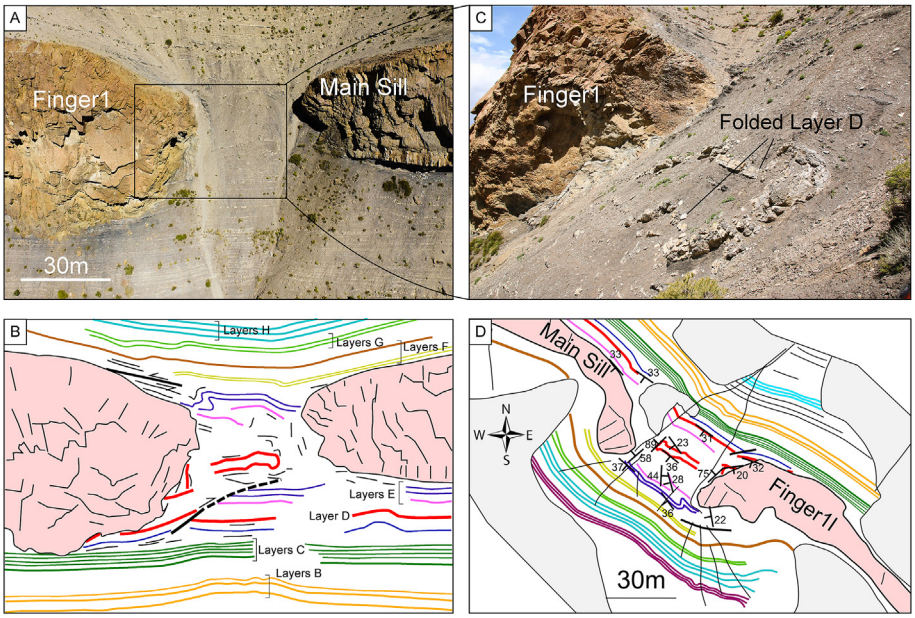

Fig. 10. A. Drone photograph of NW edge of Finger1, edge of Main Sill and host rock in between, above and below. B. Interpreted geological drawing of photograph of A. Interpreted layers are same as in Figs. 5 and 7. C. Detailed field photograph of intensively folded marker Layer D between NW edge of Finger1 and edge of Main Sill. D. Geological map of NW edge of Finger1, edge of Main Sill and host rock in between, above and below, displaying field structural measurements. Geological map is detail of Fig. 7.

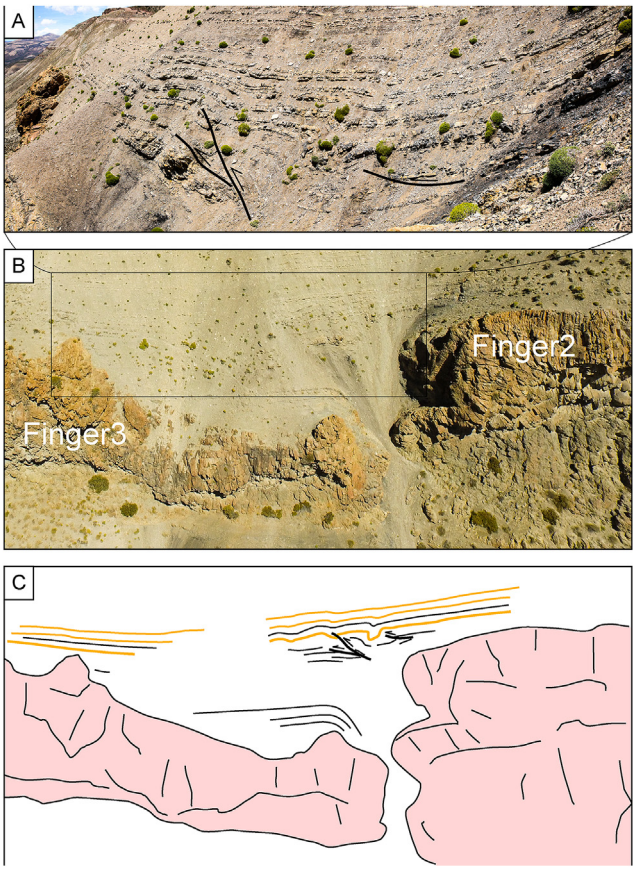

Fig. 11. A. Field photograph of host rock structures above NW edge of Finger3 and SE edge of Finger2 (see location in B). B. Drone photograph of NW edge of Finger3, SE edge of Finger2 and host rock in between and above. C. Interpreted geological drawing of photograph of B. Interpreted layers are same as in Figs. 5 and 7.

suggest that the fingers are overall tube-like structures. Their sections, as exposed along the outcrop, can exhibit variable shapes, from simple squared high thickness-to-width aspect ratio ellipses (Finger1 and Finger2) to complex low thickness-to-width aspect ratio sections (Finger3, Main Sill)(Fig. 5). The interpreted long axes of these inferred tube structures trend SW, i.e. similar to the average dip direction of the host rock layering. We cannot rule out, however, that the tube-like structures exhibit irregularities in the third dimension, as often highlighted on seismic data (Thomson and Hutton, 2004; Schofield et al., 2015).

The numerous slickensides measured on the intrusions' contacts are evidence of relative displacement between the intrusive bodies and their host rock. The key question is whether these slickensides are related to regional tectonics or not. Several elements allow us to address this question.

The measured slickensides provide an overall NE-SW movement, i.e. parallel to the fingers' inferred axes (Fig. 9). If these slickensides were of tectonic origin, we expect them to provide a consistent distribution of movement directions compatible with a dominant tectonic transport. However, this is not the case, as slickensides at the top contacts of Finger3 indicate a top-to-the-SW movement (i.e. magma to NE), whereas slickensides at the bottom contacts of Finger2 and Finger3 indicate an opposite, top-to-the-NE movement (i.e. also magma to NE). We interpreted such opposite kinematics as a magma flow marker within the fingers toward the NE (Fig. 12). These brittle slickenside structures suggest that the magma in contact with the host rock behaved brittly while the magma kept flowing viscously inside the fingers. The viscous drag of the flowing magma entrained the solidified magma, which slipped along the intrusions' contacts, leading to the formation of the brittle slickensides. The first-order consistency between the inferred fingers' axes and the kinematic flow indicators suggest that these latter are relevant markers for magma flow direction (Fig. 13).

We note, however, some variability of the orientations of the kinematic flow indicators, in particular at the edge of the Mains Sill, at the SE edge of Finger2, and locally at the bottom and top contacts of Finger3. This suggests that magma flow within the fingers was not a simple laminar flow parallel to the fingers' axes, and that some perturbation and probably some churning might have affected the magma flow.

The undulating intrusive contacts at the edges of Finger2 and the Main Sill look like closed-packed cylinders (Fig. 8), whose axes are parallel to the fingers' inferred axes and to the inferred dominant magma flow direction (Fig. 12). We infer that these undulations are also structural markers of magma flow direction during emplacement. Nevertheless, we have no clear evidence of how these undulations were formed.

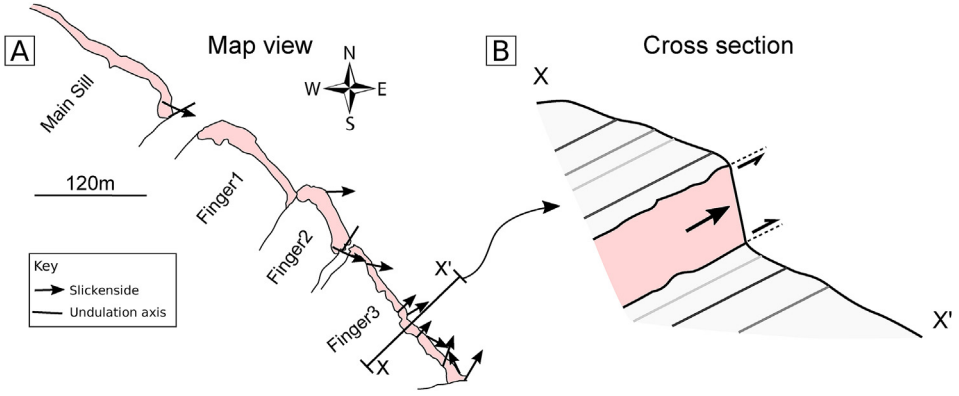

Fig. 12. A. Map view drawing of the studied fingers and the sill with the interpreted magma flow indicators measured at the contacts of the intrusions. B. Schematic cross section of Finger3 along profile X-X′ located in A, showing opposite kinematic indicators measured at top and bottom contacts.

4.3. Finger emplacement processes

The relationship between the fingers' shapes and the structures in the host rock reveals the details of magma emplacement (Pollard et al., 1975; Duffield et al., 1986; Schofield et al., 2012a; Spacapan et al., 2017). The outcrop described in this contribution is exceptional, as it displays the shapes of the intrusive units, the cooling joint patterns, magma flow indicators along the intrusions' contacts and the structures that show how the host rock accommodated the emplacement of the intrusions.

The dominant kinematics measured in the host rock is related to compression (Figs. 10 and 11), which can be locally extreme, with duplications of some host rock layers. Such compressional structures are not compatible with established tensile opening models of igneous sill and laccolith emplacement, which assume propagation controlled by local tensile stresses at the intrusion's tip (Menand, 2008; Bunger and Cruden, 2011; Galland and Scheibert, 2013). In order to explain this apparent contradiction, the relation between the fingers, their

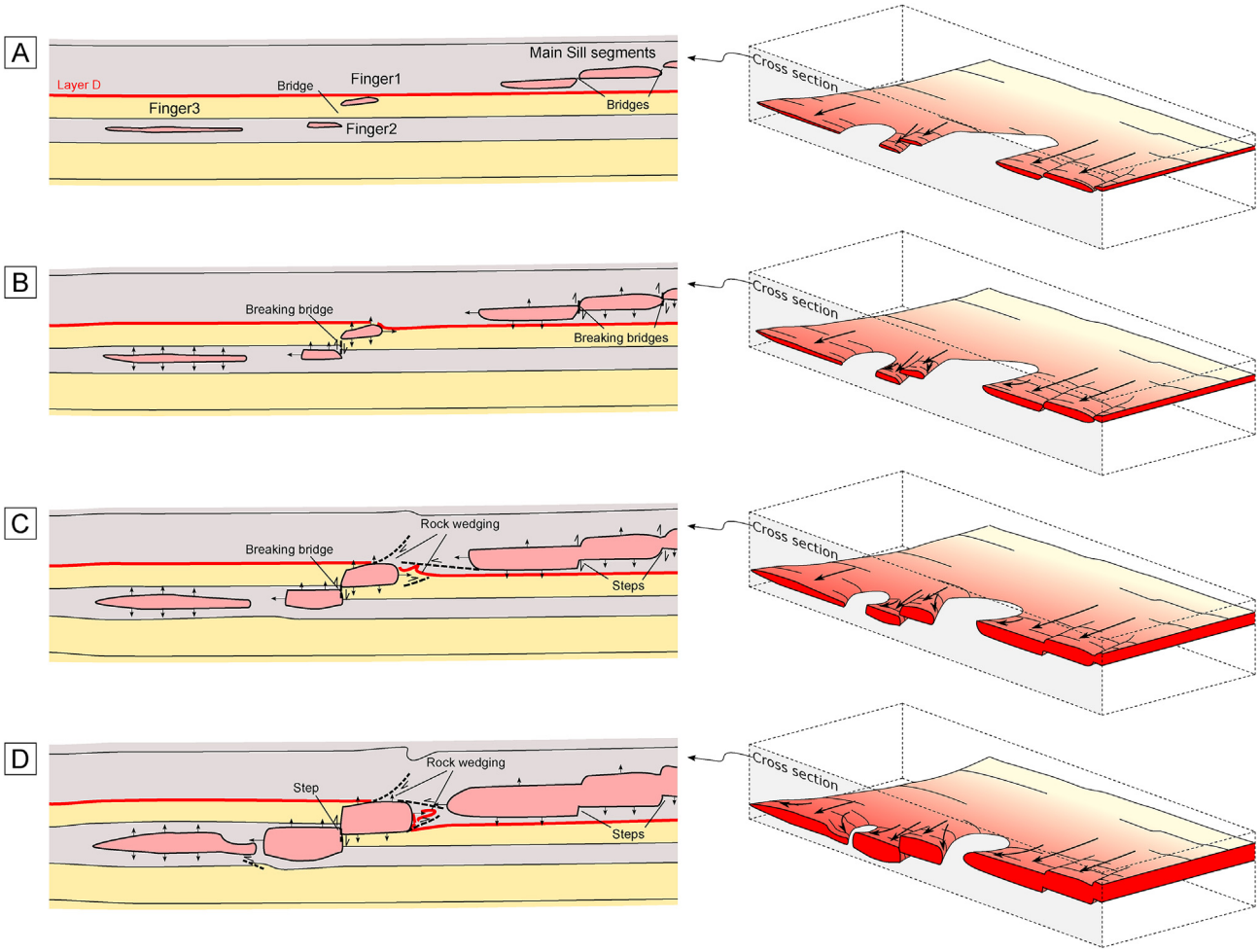

Fig. 13. Schematic 3D block diagram (right) and corresponding cross sections (left) drawings of the emplacement scenario of the studied sill and fingers. See text for detailed explanation and interpretation.

neighbouring intrusions and the structures in the host rock structure is now examined.

The sub-vertical contact between Finger1 and Finger2 is remarkable (Fig. 6A). In addition, Layers C just below Finger1 are offset vertically, relative to their position by Finger1. We infer from this observation that Finger1 and Finger2 originated as two small, thin fingers emplaced at different levels, above Layers C and below Layers B, respectively, with a bridge between them (Fig. 13A). The vertical contact between Finger1 and Finger2 suggests that both fingers were thickening in opposite directions during their growth, leading to a large intrusive step along a vertical plane (Fig. 13B and C).

The Main Sill appears as a continuous sheet. However, the observed steps along-strike the Main Sill suggest that it did not originate as a single intrusion. Similarly to the Finger1-Finger2 relation, the steps along the Main Sill indicate that neighbouring intrusive segments were initially emplaced at distinct stratigraphic levels, with thin steps between them (Fig. 13A). Their thickening broke the bridges, such that the sill segments coalesced to form one connected conduit with a stepped morphology. The linkage of the initial segments leading to the Main Sill is likely due to the fact that the vertical offset between the initial segments was smaller than that between the initial Finger1 and Finger 2 (Fig. 13A).

The Layer D crops out above Finger1 and below the Main Sill, showing that Finger1 was initially emplaced at a lower stratigraphic level than the initial Main Sill (Fig. 13A). However, these two units now appear at the same elevation on the mountain flank (Fig. 5), suggesting a relative downward thickening of the Main Sill with respect to Finger1. Note that if only relative inflation between these two units were happening, we would expect a similar type of contact as that between Finger1 and Finger2. However, the intense shortening between the Main Sill and Finger1, and between Finger2 and Finger3, shows that significant lateral propagation occurred between the edges of the Main Sill and Finger1 (see Fig. 13). This suggests that part of the magma flow near the edges was oblique to the interpreted fingers' axes (Fig. 13B–D). Such inferred out-of-axis magma flow is compatible with the kinematic indicators observed above the edge of the Main Sill, indicating magma flow towards Finger1 (Fig. 12A). The converging propagations of the edges of the Main Sill and of Finger1 led to intense shortening of the host rock, leading to rock wedging of opposite directions (Fig. 13). Similar relations between host rock shortening and kinematic indicator above the SE edge of Finger2 (Figs. 11 and 12) also suggests lateral flow toward Finger3 during the growth of Finger2 (Fig. 13B–D).

Our observations allow us to address a key question of magma emplacement regarding the relative timing of the lateral propagation of the fingers' edges versus the inflation of the fingers. The contact between Finger1 and Finger2 can be explained only by relative vertical displacements between their bottom and top contacts, and so is clearly related to inflation only. However, the intense shortening between the Main Sill and Finger1, and between Finger2 and Finger3, shows significant lateral propagation during, or after, the inflation of the fingers (see Fig. 13). We thus infer that the lateral propagation of the fingers' edges and the inflation of the fingers were coeval.

The emplacement mechanism of Finger3 is difficult to constrain, because the host rock does not crop out well. The shape of its NW edge suggests a similar propagation mechanism as those described above (Fig. 11). However, its irregular morphology with respect to those of Finger1, Finger2 and the Main Sill suggests a more complex emplacement mechanism. In addition, the variable orientations of the slickensides measured on its top and bottom contacts (Fig. 9) indicate variable magma flow directions during its growth (Fig. 12). Note that Finger3 represents the extreme edge of the studied intrusive complex. We infer that magma flow at the edges of large sills is more chaotic than magma flow in the internal parts of the sill due to cooling effects, i.e. the magma near the tip of the intrusion is colder, and so exhibits a higher viscosity, which can lead to a complex intrusion shape (Chanceaux and Menand, 2016).

5. Discussion

5.1. Implications for magma emplacement processes

The overall shape of the intrusion described in this paper is that of a dominantly concordant magmatic sheet, i.e. a sill (Galland et al., 2018), which extends over several kilometres to the west and south of the studied outcrop. However, our detailed observations show that it did not result from the emplacement of a single sheet, but from the coalescence of numerous smaller individual intrusive segments of likely dominant finger shapes (Fig. 13). The emplacement of this intrusion cannot have been achieved in the ways inferred from the established sill emplacement models, which consider a sill as a single continuous sheet of low thickness-to-width and thickness-to-length aspect ratios and of regular and simple periphery (e.g., Bunger and Cruden, 2011; Galland and Scheibert, 2013; Cruden et al., 2018). In contrast, the emplacement of this sill appears to be related to emplacement of distinct intrusive units that coalescence (Fig. 13), resulting in a complex-shaped periphery (e.g., Pollard et al., 1975; Delaney and Pollard, 1981; Thomson and Hutton, 2004).

Each intrusive unit is exposed on a broadly planar outcrop, which provides a 2D section across the inferred long dimension of the overall sheet and associated fingers. The units in cross section exhibit rounded, blunt and irregular edges, very low thickness-to-width aspect ratios, and parallel upper and lower contacts. In addition, all structures in the host rock adjacent to the intrusions' edges reflect shortening. These observations are in agreement with viscoelastic fingering mechanisms produced in the laboratory experiments of Bertelsen et al. (2018), i.e. the viscous magma indents its host rocks, causing it to deform by ductile flow or shear failure. Our observations are also in agreement with the viscous indenter model in a brittle and ductile host rock (Pollard, 1973; Mathieu et al., 2008; Abdelmalak et al., 2012), suggesting that the viscoelastic fingering and the viscous indenter models are closely related. Conversely, all these observations are at odds with established models of tensile fracturing of an elastic host rock (e.g., Pollard and Johnson, 1973; Kavanagh et al., 2006; Maccaferri et al., 2011), which assume sharp edges and wedge-shape intrusions. We cannot rule out, however, that early tensile fracturing accommodated the initial emplacement, and that the associated structures have been obliterated by the subsequent, substantial inelastic deformation. Our observations are very similar to those of Spacapan et al. (2017) made for a much smaller intrusion (0.5–1 m thick). We therefore suggest that the viscoelastic fingering/viscous indenter emplacement mechanisms operate on several scales of volcanic plumbing systems.

Since the main magma flow direction is perpendicular to the studied outcrop (Fig. 12), the observed compressional structures in the host rock only accommodate the lateral propagation of the fingers (Fig. 13). The extent to which this mechanism accommodates the propagation of the intrusions parallel to the flow direction is not visible on this outcrop. Nevertheless, the very low thickness-to-width aspect ratios of the intrusive units can hardly be explained by tensile elastic fracturing. This suggests that a similar pushing mechanism accommodated the propagation of the intrusion in all directions.

All the observed structures in the host rock indicate that the lateral propagation of the intrusions' edges was accommodated by inelastic deformation, i.e. brittle shear failure and ductile shearing. These structures are very similar to those observed in the 2-dimensional experiments of Abdelmalak et al. (2012). Our observations show that the inelastic properties of the Earth's crust are first-order parameters for the emplacement mechanism of magma, especially when the host rock is weak. This conclusion supports the interpretations of the laboratory models of Schmiedel et al. (2017a), Guldstrand et al. (2017) and Guldstrand et al. (2018), and the numerical models of Haug et al. (2017) and Haug et al. (2018), which suggest that the Coulomb properties of the Earth's crust play a major role in the propagation and emplacement of igneous sheet intrusions.

One can argue that the shale host rock of the studied outcrop is very weak and is not representative of many crustal or sedimentary rocks, thus questioning the widespread applicability of our conclusions. For example, Duffield et al. (1986) described similar structures accommodating the emplacement of igneous fingers in shallow, poorly consolidated sediments. Nevertheless, most igneous intrusions in the Neuquén Basin, for instance, were emplaced in the organic-rich shale formations of the basin (e.g., Rodriguez Monreal et al., 2009; Galland et al., 2018; Rabbel et al., 2018; Spacapan et al., 2018; Spacapan et al., 2019). In many other basins, sills are also emplaced in organic-rich shale formations (Svensen et al. 2004, 2007; Jackson et al., 2013). In addition, 3D seismic data of igneous sill-complexes show that sills dominantly exhibit lobate morphologies interpreted as coalesced fingers similar to those described in this paper (e.g., Thomson and Hutton, 2004; Schofield et al., 2012a). We therefore infer that the conclusions of our field study likely apply to numerous sills worldwide.

The numerous slickensides at the intrusions' contacts, interpreted as flow indicators, indicate that brittle deformation of the magma partly accommodated the emplacement of the fingers at Las Loicas. This suggests that at the intrusion contacts, the magma was cold enough to behave in brittle manner, whereas the central parts of the fingers were still likely liquid and flowing. Similar observations have been documented at the Sandfell rhyolitic laccolith, Iceland (Mattsson et al., 2018). Our observations also support the assumptions of the laboratory models of Chanceaux and Menand (2014) and Chanceaux and Menand (2016), who studied the effects of magma cooling on sill emplacement in laboratory models. Finally, the opposite brittle kinematic indicators observed on the intrusions' contacts are in agreement with the seismological observations monitored during the emplacement of a basaltic dyke in Iceland (White et al., 2011).

This paper describes macro-structures in the host rock (folding, faulting, etc) related to the emplacement of the fingers. Other micro-scale mechanisms such as porosity reduction/collapse, pressure/solution and deformation bands have been inferred to partly accommodate the emplacement of, e.g. the Trachyte Mesa intrusion, Henry Mountains, Utah (Morgan et al., 2008; Wilson et al., 2016). However, the host rock of the Trachyte Mesa intrusion is sandstone, and these latter mechanisms are typically observed within deformed sandstone. Conversely, the host rock in this study is made of shale and thin carbonate layers, where initial porosity is low and deformation bands unlikely. We therefore suggest that the emplacement of the studied intrusions was dominantly controlled by the described macro-structures.

5.2. Structural criteria for magma-flow direction indicators

In the literature, the long axes of igneous fingers have been interpreted in terms of magma-flow indicators for sill and dyke emplacement, both for outcrop and subsurface seismic data (Hansen and Cartwright, 2006a; Thomson, 2007; Schofield et al., 2012b; Schmiedel et al., 2017b; Magee et al., 2018). Stepped morphology of sills and dykes has also been interpreted as a structural marker of the dominant magma flow direction (Smith, 1987; Hutton, 2009; Healy et al., 2018; Magee et al., 2018). On a smaller scale, shape preferred orientation of minerals in the magmatic rock has also been used as magma flow indicator (Hoyer and Watkeys, 2017). Recently, Westerman et al. (2018, and references therein) also documented kinematic indicators at the intrusion's contacts. Thanks to the full 3D reconstructions of igneous fingers on seismic data, it is possible to infer the magma flow directions, commonly from the centres to the margins of the sills (Schofield et al., 2015; Magee et al., 2016; Schmiedel et al., 2017b). However, outcrops of igneous fingers usually only expose small parts of magma fingers, which make it challenging to infer magma flow directions through the fingers.

Our structural observations bring such exciting new insights. The consistency between the interpreted fingers' long axes, perpendicular to the outcrop, and the kinematic indicators observed at the fingers' contacts strongly suggests that the dominant magma flow direction at the Las Loicas sills was from SW to NE. These structural observations suggest that they are likely reliable indicators of magma flow directions through fingers.

The slickenside kinematic indicators measured at the intrusions' contacts highlight locally complex magma flow distribution within the fingers, with a significant component not parallel to the interpreted fingers' long axes. Such off-axis magma flow is responsible for the lateral propagation of the fingers, shortening of the host rock squeezed between fingers, and eventually for finger linkage. Local magma flow is thus critical for revealing the details of fingers and sills emplacement, as suggested by measurement of complex flow patterns in the laboratory models of Kavanagh et al. (2018).

The formation of the slickensides observed at the fingers' contacts can have two explanations. First, the rapid cooling of the magma at the contact can lead to significant viscosity increase (e.g., Chanceaux and Menand, 2016; Thorey and Michaut, 2016), such that it becomes brittle. Second, the shear rates experienced by the magma at the contacts are expected to be much higher than in the inner parts of the fingers. Cordonnier et al. (2012) and Pistone et al. (2015) show that a magma can fail in a brittle fashion at high shear rates, while it can flow viscously at lower shear rates, as observed in volcanic conduits. This suggests that the near-contact brittle features observed in the studied intrusive complex can show that the magma locally crossed the brittle-ductile transition as a result of higher shear rates. Such shear-controlled mechanism, however, is likely to occur dominantly for felsic magmas, such as at the studied outcrop, rather that for mafic magmas (Pistone et al., 2015).

5.3. Implications for seismic interpretation of igneous fingers and fluid flow

Numerous sills imaged on seismic data exhibit characteristic lobate morphology, suggesting that they result from the emplacement of coalesced igneous fingers (Hansen and Cartwright, 2006a; Thomson, 2007; Schofield et al., 2012b; Schmiedel et al., 2017b). The resolution of seismic data does not allow the imaging of the host rock's structures that accommodated the emplacement of the sills. Our detailed, standard outcrop-scale, field observations applied on an exceptional seismic-scale outcrop have the potential to considerably advance the structural interpretation of seismic data imaging igneous sills, as discussed by Rabbel et al. (2018).

In volcanic basins, igneous sills strongly impact fluid flow within their host sedimentary sequences, with tremendous potential implications for petroleum systems (Rateau et al., 2013; Senger et al. 2015, 2017; Spacapan et al. 2018, 2019) and aquifers (Chevallier et al., 2001). The sills themselves are affected by numerous fractures due to magma cooling, and the emplacement of the sills produce fractures and damage in the host rock. However, the small scale of emplacement-induced fracturing and damage is below seismic resolution (Rabbel et al., 2018), such that assessing the full structural impact of igneous sills on fluid flow using seismic data is impossible. Our field study provides valuable structural insights (at sub-seismic scales), as we show that significant fracturing and damage mostly concentrate in between fingers and at the vicinity of steps. These are features that can be mapped on 3D seismic data thus can potentially be used as a proxy for damage. A more focussed structural study is now necessary to quantify fracture and damage properties (density, opening, connectivity, anisotropy) to directly quantify the potential fluid flow implications of igneous sills in basin models.

6. Conclusions

In this paper, we report on detailed structural observations of an exhumed igneous sill consisting of fingers emplaced in Mesozoic organic-rich shale. We combine drone survey photography with direct

outcrop measurements to reveal the emplacement mechanisms of the intrusive complex. The conclusions of our study are listed below.

- The sill is made of segments emplaced at distinct stratigraphic levels. These segments subsequently grew, either inflating to distinct fingers, or coalescing to a stepped sill.
- Sharp vertical contacts between fingers could incorrectly be interpreted as tectonic fault offsets, however we demonstrate that they are in fact emplacement features and result from the coalescence of fingers.
- The segmented nature of the intrusion shows that its overall sheet shape does not result from the emplacement of a single sheet, as assumed by most models, but from the coalescence of fingers.
- The edges of the fingers are blunt and their propagation occurred by pushing aside the host rock, leading to intense shortening, rock wedging, and even squeezing of the host rock in between the fingers. This mechanism is in agreement with the viscoelastic fingering and viscous indenter models. This shows that the inelastic properties of crustal rocks are of primary importance on the emplacement of magma intrusions in the shallow brittle crust.
- Brittle slickensides observed at the intrusion's contacts are interpreted as indicators of local magma flow in the cooled chilled margin, while the interior of the intrusion was still molten and flowing.
- The consistency between the brittle kinematic indicators observed at the contacts and the fingers' axes confirm that these kinematic indicators are reliable for inferring magma flow direction during emplacement.
- Our small-scale structural observations carried out on a seismic-scale outcrop should considerably aid the structural interpretation of seismic data imaging igneous sills, filling the gap between outcrop-scale field observations and seismic-scale geophysical data.

Our study highlights the necessity and value of integrating field measurements with drone survey of large outcrops, in order to ground truth the remote observations.

Acknowledgments

Spacapan's salary is covered by a CONICET-YPF Foundation grant (Grant 2282014000359600). Rabbel's salary is covered by a Faculty of Mathematics and Natural Sciences grant at the University of Oslo. The fieldwork was partly supported by the DIPS project (grant no. 240467) funded by the Norwegian Research Council, and by YPF.

References

Abdelmalak, M.M., Mourgues, R., Galland, O., Bureau, D., 2012. Fracture mode analysis and related surface deformation during dyke intrusion: results from 2D experimental modelling. Earth Planet. Sci. Lett. 359–360, 93–105. https://doi.org/10.1016/j.epsl.2012.10.008.

Álvarez Cerimedo, J., Orts, D., Rojas Vera, E., Folguera, A., Bottesi, G., Ramos, V.A., 2013. Mecanismos y fases de construcción orogénicos del frente oriental andino (36 S, Argentina). Andean Geol. 40, 504–520.

Bertelsen, H.S., Rogers, B.D., Galland, O., Dumazer, G., Abbana Bennani, A., 2018. Laboratory modelling of coeval brittle and ductile deformation during magma emplacement into viscoelastic rocks. Front. Earth Sci. 6. https://doi.org/10.3389/feart.2018.00199.

Brissón, I., Veiga, R., 1998. La estratigrafía y estructura de la Cuenca Neuquina. Gira de campo: Buenos Aires. Repsol YPF (unpublished report).

Bunger, A.P., Cruden, A.R., 2011. Modeling the growth of laccoliths and large mafic sills: role of magma body forces. J. Geophys. Res. 116, B02203. https://doi.org/10.1029/2010jb007648.

Caminos, R., Nullo, F.E., Panza, J.L., Ramos, V.A., 1993. Mapa Geológico de la provincia de Mendoza, República Argentina.

Cartwright, J., Hansen, D.M., 2006. Magma transport through the crust via interconnected sill complexes. Geology 34, 929–932.

Chanceaux, L., Menand, T., 2014. Solidification effects on sill formation: an experimental approach. Earth Planet. Sci. Lett. 403, 79–88. https://doi.org/10.1016/j.epsl.2014.06.018.

Chanceaux, L., Menand, T., 2016. The effects of solidification on sill propagation dynamics and morphology. Earth Planet. Sci. Lett. 442, 39–50. https://doi.org/10.1016/j.epsl.2016.02.044.

Chevallier, L., Goedhart, M., Woodford, A., 2001. The Influence of Dolerite Sill and Ring Complexes on the Occurrence of Grounwater in the Karoo Fractured Aquifers: a Morpho-Tectonic Approach Report 937.

Chevallier, L., Woodford, A., 1999. Morpho-tectonics and mechanism of emplacement of the dolerite rings and sills of the western Karoo, South Africa. S. Afr. J. Geol. 102, 43–54.

Cobbold, P., Rossello, E., 2003. Aptian to recent compressional deformation, foothills of the Neuquén Basin, Argentina. Mar. Petrol. Geol. 20, 429–443.

Combina, A.M., Nullo, F., 2011. Ciclos tectónicos, volcánicos y sedimentarios del Cenozoico del sur de Mendoza-Argentina (35°-37°S y 69°30′W). Andean Geol. 38, 198–218.

Cordonnier, B., Caricchi, L., Pistone, M., Castro, J., Hess, K.-U., Gottschaller, S., Manga, M., Dingwell, D.B., Burlini, L., 2012. The viscous-brittle transition of crystal-bearing silicic melt: direct observation of magma rupture and healing. Geology 40, 611–614. https://doi.org/10.1130/g3914.1.

Cruden, A.R., McCaffrey, K.J.W., Bunger, A.P., 2018. Geometric scaling of tabular igneous intrusions: implications for emplacement and growth. In: Breitkreuz, C., Rocchi, S. (Eds.), Physical Geology of Shallow Magmatic Systems: Dykes, Sills and Laccoliths. Springer International Publishing, Cham, pp. 11–38.

Delaney, P.T., Pollard, D.D., 1981. Deformation of Host Rocks and Flow of Magma during Growth of Minette Dikes and Breccia-Bearing Intrusions Near Ship Rock, New Mexico.

Delpino, D., Deza, M., 1995. Mapa Geológico y Recursos Minerales de la Privincia del Neuquén, República Argentina.

Donnadieu, F., Merle, O., 1998. Experiments on the indentation process during cryptodome intrusions: new insights into Mount St. Helens deformation. Geology 26, 79–82.

Duffield, W.A., Bacon, C.R., Delaney, P.T., 1986. Deformation of poorly consolidated sediment during shallow emplacement of a basalt sill, Coso Range, California. Bull. Volcanol. 48, 97–107. https://doi.org/10.1007/bf01046545.

Dyhr, C.T., Holm, P.M., Llambías, E.J., 2013. Geochemical constraints on the relationship between the Miocene–Pliocene volcanism and tectonics in the Palaoco and Fortunoso volcanic fields, Mendoza Region, Argentina: new insights from 40Ar/39Ar dating, Sr–Nd–Pb isotopes and trace elements. J. Volcanol. Geotherm. Res. 266, 50–68. https://doi.org/10.1016/j.jvolgeores.2013.08.005.

Eide, C.H., Schofield, N., Jerram, D.A., Howell, J.A., 2016. Basin-scale architecture of deeply emplaced sill complexes: jameson Land, East Greenland. J. Geol. Soc. 174, 23–40. https://doi.org/10.1144/jgs2016-018.

Eide, C.H., Schofield, N., Lecomte, I., Buckley, S.J., Howell, J.A., 2017. Seismic interpretation of sill-complexes in sedimentary basins: the 'Sub-Sill imaging problem. J. Geol. Soc. 175, 193–209.

Fennell, L.M., Folguera, A., Naipauer, M., Gianni, G., Rojas Vera, E.A., Bottesi, G., Ramos, V.A., 2017. Cretaceous deformation of the southern Central Andes: synorogenic growth strata in the Neuquén Group (35 30′–37 S). Basin Res. 29, 51–72.

Folguera, A., Bottesi, G., Duddy, I., Martín-González, F., Orts, D., Sagripanti, L., Vera, E.R., Ramos, V.A., 2015. Exhumation of the Neuquén Basin in the southern Central Andes (Malargüe fold and thrust belt) from field data and low-temperature thermochronology. J. South Am. Earth Sci. 64, 381–398.

Galerne, C.Y., Galland, O., Neumann, E.R., Planke, S., 2011. 3D relationships between sills and their feeders: evidence from the Golden Valley Sill Complex (Karoo Basin) and experimental modelling. J. Volcanol. Geotherm. Res. 202, 189–199. https://doi.org/10.1016/j.jvolgeores.2011.02.006.

Galland, O., Bertelsen, H.S., Eide, C.H., Guldstrand, F., Haug, Ø.T., Leanza, H.A., Mair, K., Palma, O., Planke, S., Rabbel, O., Rogers, B.D., Schmiedel, T., Souche, A., Spacapan, J.B., 2018. Storage and transport of magma in the layered crust-Formation of sills and related flat-lying intrusions. In: Burchardt, S. (Ed.), Volcanic and Igneous Plumbing Systems. Elsevier, pp. 111–136.

Galland, O., Scheibert, J., 2013. Analytical model of surface uplift above axisymmetric flat-lying magma intrusions: implications for sill emplacement and geodesy. J. Volcanol. Geotherm. Res. 253, 114–130. https://doi.org/10.1016/j.jvolgeores.2012.12.006.

Giambiagi, L., Alvarez, P.P., Bechis, F., Tunik, M., 2005. Influencia de las estructuras de rift triásico-jurásicas sobre el estilo de deformación en las fajas plegadas y corridas de Aconcagua y Malargüe, Mendoza. Rev. Asoc. Geol. Argent. 60, 662–671.

Guldstrand, F., Burchardt, S., Hallot, E., Galland, O., 2017. Dynamics of surface deformation induced by dikes and cone sheets in a cohesive Coulomb brittle crust. J. Geophys. Res. Solid Earth 122, 8511–8524. https://doi.org/10.1002/2017JB014346.

Guldstrand, F., Galland, O., Hallot, E., Burchardt, S., 2018. Experimental constraints on forecasting the location of volcanic eruptions from pre-eruptive surface deformation. Front. Earth Sci. 6. https://doi.org/10.3389/feart.2018.00007.

Hansen, D.M., Cartwright, J.A., 2006a. Saucer-shaped sill with lobate morphology revealed by 3D seismic data: implications for resolving a shallow-level sill emplacement mechanism. J. Geol. Soc. Lond. 163, 509–523.

Hansen, D.M., Cartwright, J.A., 2006b. The three-dimensional geometry and growth of forced folds above saucer-shaped igneous sills. J. Struct. Geol. 28, 1520–1535.

Haug, Ø.T., Galland, O., Souloumiac, P., Souche, A., Guldstrand, F., Schmiedel, T., 2017. Inelastic damage as a mechanical precursor for the emplacement of saucer-shaped intrusions. Geology 45, 1099–1102. https://doi.org/10.1130/G39361.1.

Haug, Ø.T., Galland, O., Souloumiac, P., Souche, A., Guldstrand, F., Schmiedel, T., Maillot, B., 2018. Shear versus tensile failure mechanisms induced by sill intrusions – Implications for emplacement of conical and saucer-shaped intrusions. J. Geophys. Res. Solid Earth 123, 3430–3449. https://doi.org/10.1002/2017JB015196.

Healy, D., Rizzo, R.E., Duffy, M., Farrell, N.J.C., Hole, M.J., Muirhead, D., 2018. Field evidence for the lateral emplacement of igneous dykes: implications for 3D mechanical models and the plumbing beneath fissure eruptions. Volcanica 1, 85–105.

https://doi.org/10.30909/vol.01.02.85105.
Horsman, E., Tikoff, B., Morgan, S.S., 2005. Emplacement-related fabric and multiple sheets in the Maiden Creek sill, Henry mountains, Utah, USA. J. Struct. Geol. 27, 1426–1444. https://doi.org/10.1016/j.jsg.2005.03.003.
Horton, B.K., Fuentes, F., Boll, A., Starck, D., Ramirez, S.G., Stockli, D.F., 2016. Andean stratigraphic record of the transition from backarc extension to orogenic shortening: a case study from the northern Neuquén Basin, Argentina. J. South Am. Earth Sci. 71, 17–40. https://doi.org/10.1016/j.jsames.2016.06.003.
Howell, J.A., Schwarz, E., Spalletti, L.A., Veiga, G.D., 2005. The Neuquén Basin: an Overview, vol. 252. Geological Society, London, Special Publications, pp. 1–14.
Hoyer, L., Watkeys, M.K., 2017. Using magma flow indicators to infer flow dynamics in sills. J. Struct. Geol. 96, 161–175. https://doi.org/10.1016/j.jsg.2017.02.005.
Hutton, D.H.W., 2009. Insights into magmatism in volcanic margins: bridge structures and a new mechanism of basic sill emplacement, Theron Mountains, Antarctica. Petrol. Geosci. 15, 269–278. https://doi.org/10.1144/1354-079309-841.
Jackson, C.A.L., Schofield, N., Golenkov, B., 2013. Geometry and controls on the development of igneous sill-related forced-folds: a 2D seismic reflection case study from offshore southern Australia. Geol. Soc. Am. Bull. 125, 1874–1890.
Jerram, D.A., Davis, G.R., Mock, A., Charrier, A., Marsh, B.D., 2010. Quantifying 3D crystal populations, packing and layering in shallow intrusions: a case study from the Basement Sill, Dry Valleys, Antarctica. Geosphere 6, 537–548. https://doi.org/10.1130/GES00538.1.
Kavanagh, J.L., Burns, A.J., Hilmi Hazim, S., Wood, E.P., Martin, S.A., Hignett, S., Dennis, D.J.C., 2018. Challenging dyke ascent models using novel laboratory experiments: implications for reinterpreting evidence of magma ascent and volcanism. J. Volcanol. Geotherm. Res. 354, 87–101. https://doi.org/10.1016/j.jvolgeores.2018.01.002.
Kavanagh, J.L., Menand, T., Sparks, R.S.J., 2006. An experimental investigation of sill formation and propagation in layered elastic media. Earth Planet. Sci. Lett. 245, 799–813.
Kozlowski, E., Manceda, R., Ramos, V., Ramos, V., 1993. Geología y Recursos Naturales de Mendoza: Relatorio del 12 congreso Geológico Argentino y 2 Congreso de Exploración de Hidrocarburos. Estructura I (18), 235–256.
Maccaferri, F., Bonafede, M., Rivalta, E., 2011. A quantitative study of the mechanisms governing dike propagation, dike arrest and sill formation. J. Volcanol. Geotherm. Res. 208, 39–50. https://doi.org/10.1016/j.jvolgeores.2011.09.001.
Magee, C., Hunt-Stewart, E., Jackson, C.A.L., 2013. Volcano growth mechanisms and the role of sub-volcanic intrusions: insights from 2D seismic reflection data. Earth Planet. Sci. Lett. 373, 41–53. https://doi.org/10.1016/j.epsl.2013.04.041.
Magee, C., Jackson, C.A.L., Schofield, N., 2014. Diachronous sub-volcanic intrusion along deep-water margins: insights from the Irish Rockall Basin. Basin Res. 26, 85–105. https://doi.org/10.1111/bre.12044.
Magee, C., Muirhead, J.D., Karvelas, A., Holford, S.P., Jackson, C.A.L., Bastow, I.D., Schofield, N., Stevenson, C.T.E., McLean, C., McCarthy, W., Shtukert, O., 2016. Lateral magma flow in mafic sill complexes. Geosphere 12, 809–841. https://doi.org/10.1130/ges01256.1.
Magee, C., Muirhead, J.D., Schofield, N., Walker, R.J., Galland, O., Holford, S.P., Spacapan, J.B., Jackson, C.A.L., McCarthy, W., 2018. Structural signatures of igneous sheet intrusion propagation. J. Struct. Geol. https://doi.org/10.1016/j.jsg.2018.07.010.
Mathieu, L., van Wyk de Vries, B., Holohan, E.P., Troll, V.R., 2008. Dykes, cups, saucers and sills: analogue experiments on magma intrusion into brittle rocks. Earth Planet. Sci. Lett. 271, 1–13.
Mattsson, T., Burchardt, S., Almqvist, B.S.G., Ronchin, E., 2018. Syn-emplacement fracturing in the Sandfell laccolith, eastern Iceland—implications for rhyolite intrusion growth and volcanic hazards. Front. Earth Sci. 6. https://doi.org/10.3389/feart.2018.00005.
Menand, T., 2008. The mechanics and dynamics of sills in layered elastic rocks and their implications for the growth of laccoliths and other igneous complexes. Earth Planet. Sci. Lett. 267, 93–99.
Merle, O., Donnadieu, F., 2000. Indentation of volcanic edifices by the ascending magma. In: Vendeville, B., Mart, Y., Vigneresse, J.-L. (Eds.), Salt, Shale and Igneous Diapirs in and Around Europe. Geological Society, London, Special Publications, Geological Society, London, Special Publications, pp. 43–53.
Michaut, C., 2011. Dynamics of magmatic intrusions in the upper crust: theory and applications to laccoliths on Earth and the Moon. J. Geophys. Res. 116, B05205. https://doi.org/10.1029/2010jb008108.
Monreal, F.R., Villar, H., Baudino, R., Delpino, D., Zencich, S., 2009. Modeling an atypical petroleum system: a case study of hydrocarbon generation, migration and accumulation related to igneous intrusions in the Neuquen Basin, Argentina. Mar. Petrol. Geol. 26, 590–605.
Morgan, S.S., Stanik, A., Horsman, E., Tikoff, B., de Saint Blanquat, M., Habert, G., 2008. Emplacement of multiple magma sheets and wall rock deformation: Trachyte Mesa intrusion, Henry Mountains, Utah. J. Struct. Geol. 30, 491–512. https://doi.org/10.1016/j.jsg.2008.01.005.
Muirhead, J.D., Airoldi, G., Rowland, J.V., White, J.D.L., 2012. Interconnected sills and inclined sheet intrusions control shallow magma transport in the Ferrar large igneous province, Antarctica. Geol. Soc. Am. Bull. 124, 162–180. https://doi.org/10.1130/b30455.1.
Muirhead, J.D., Airoldi, G., White, J.D.L., Rowland, J.V., 2014. Cracking the lid: sill-fed dikes are the likely feeders of flood basalt eruptions. Earth Planet. Sci. Lett. 406, 187–197. http://doi.org/10.1016/j.epsl.2014.08.036.
Nase, J., Lindner, A., Creton, C., 2008. Pattern formation during deformation of a confined viscoelastic layer: from a viscous liquid to a soft elastic solid. Phys. Rev. Lett. 101, 074503. https://doi.org/10.1103/PhysRevLett.101.074503.
Orts, D.L., Folguera, A., Giménez, M., Ramos, V., 2012. Variable structural controls through time in the southern central Andes (~ 36°S). Andean Geol. 39, 220–241.
Petford, N., Cruden, A.R., McCaffrey, K.J.W., Vigneresse, J.L., 2000. Granite magma formation, transport and emplacement in the Earth's crust. Nature 408, 669–673.
Pistone, M., Cordonnier, B., Caricchi, L., Ulmer, P., Marone, F., 2015. The viscous to brittle transition in crystal- and bubble-bearing magmas. Front. Earth Sci. 3. https://doi.org/10.3389/feart.2015.00071.
Planke, S., Rasmussen, T., Rey, S.S., Myklebust, R., 2005. Seismic characteristics and distribution of volcanic intrusions and hydrothermal vent complexes in the Vøring and Møre basins. In: Doré, A.G., Vining, B.A. (Eds.), Proc. 6th Petrol. Geol. Conf. Geological Society, London.
Pollard, D.D., 1973. Derivation and evaluation of a mechanical model for sheet intrusions. Tectonophysics 19, 233–269. https://doi.org/10.1016/0040-1951(73)90021-8.
Pollard, D.D., Johnson, A.M., 1973. Mechanics of growth of some laccolithic intrusions in the Henry Mountains, Utah, II. Bending and failure of overburden layers and sill formation. Tectonophysics 18, 311–354.
Pollard, D.D., Muller, O.H., Dockstader, D.R., 1975. The form and growth of fingered sheet intrusions. Geol. Soc. Am. Bull. 86, 351–363. https://doi.org/10.1130/0016-7606(1975)86<351:tfagof>2.0.co;2.
Polteau, S., Ferré, E.C., Planke, S., Neumann, E.-R., Chevallier, L., 2008. How are saucer-shaped sills emplaced? Constraints from the Golden valley sill, South Africa. J. Geophys. Res. 113. https://doi.org/10.1029/2008JB005620.
Poppe, S., Holohan, E.P., Galland, O., Buls, N., van Gompel, G., Keelson, B., Tournigand, P.-Y., Brancart, J., Hollis, D., Nila, A., Kervyn, M., 2019. An inside perspective on magma intrusion: quantifying 3D displacement and strain in laboratory experiments by dynamic X-Ray computed tomography. Front. Earth Sci. 7. https://doi.org/10.3389/feart.2019.00062.
Rabbel, O., Galland, O., Mair, K., Lecomte, I., Senger, K., Spacapan, J.B., Manceda, R., 2018. From field analogues to realistic seismic modelling: a case study of an oil-producing andesitic sill complex in the Neuquén Basin, Argentina. J. Geol. Soc. https://doi.org/10.1144/jgs2017-116.
Ramos, V.A., Vujovich, G., Martino, R., Otamendi, J., 2010. Pampia: a large cratonic block missing in the Rodinia supercontinent. J. Geodyn. 50, 243–255.
Rateau, R., Schofield, N., Smith, M., 2013. The potential role of igneous intrusions on hydrocarbon migration, West of Shetland. Petrol. Geosci. 19, 259–272. https://doi.org/10.1144/petgeo2012-035.
Rodriguez Monreal, F., Villar, H.J., Baudino, R., Delpino, D., Zencich, S., 2009. Modeling an atypical petroleum system: a case study of hydrocarbon generation, migration and accumulation related to igneous intrusions in the Neuquén Basin, Argentina. Mar. Petrol. Geol. 26, 590–605. https://doi.org/10.1016/j.marpetgeo.2009.01.005.
Rossello, E.A., Cobbold, P.R., Diraison, M., Arnaud, N., 2002. Auca Mahuida (Neuquén Basin, Argentina): A Quaternary Shield Volcano on a Hydrocarbon-Producing Substrate. 5th ISAG, *Extended Abstracts*, Toulouse, pp. 549–552.
Rubin, A.M., 1995. Propagation of magma-filled cracks. Annu. Rev. Earth Planet Sci. 23, 287–336.
Saffman, P.G., Taylor, G., 1958. The penetration of a fluid into a porous medium or Hele-Shaw cell containing a more viscous liquid. Proc. Roy. Soc. Lond. Ser. A Math. Phys. Sci. 245, 312–329. https://doi.org/10.1098/rspa.1958.0085.
Scheibert, J., Galland, O., Hafver, A., 2017. Inelastic deformation during sill and laccolith emplacement: insights from an analytic elasto-plastic model. J. Geophys. Res. Solid Earth 122, 923–945. https://doi.org/10.1002/2016JB013754.
Schiuma, M.F., 1994b. Intrusivos del valle del Río Grande, provincia de Mendoza, su importancia como productores de hidrocarburos. Facultad de Ciencias Naturales y Museo.
Schmiedel, T., Galland, O., Breitkreuz, C., 2017a. Dynamics of sill and laccolith emplacement in the brittle crust: role of host rock strength and deformation mode. J. Geophys. Res. Solid Earth 122, 8625–9484. https://doi.org/10.1002/2017JB014468.
Schmiedel, T., Kjoberg, S., Planke, S., Magee, C., Galland, O., Schofield, N., Jackson, C.A.-L., Jerram, D.A., 2017b. Mechanisms of overburden deformation associated with the emplacement of the Tulipan sill, mid-Norwegian margin. Interpretation 5, SK23–SK38. https://doi.org/10.1190/int-2016-0155.1.
Schofield, N., Brown, D.J., Magee, C., Stevenson, C.T., 2012a. Sill morphology and comparison of brittle and non-brittle emplacement mechanisms. J. Geol. Soc. 169, 127–141. https://doi.org/10.1144/0016-76492011-078.
Schofield, N., Heaton, L., Holford, S.P., Archer, S.G., Jackson, C.A.L., Jolley, D.W., 2012b. Seismic imaging of "broken bridges": linking seismic to outcrop-scale investigations of intrusive magma lobes. J. Geol. Soc. 169, 421–426. https://doi.org/10.1144/0016-76492011-150.
Schofield, N., Holford, S.P., Millett, J., Brown, D.J., Jolley, D., Passey, S.R., Muirhead, D., Grove, C., Magee, C., Murray, J., Hole, M., Jackson, C.A.L., Stevenson, C.T., 2015. Regional magma plumbing and emplacement mechanisms of the Faroe-Shetland Sill Complex: implications for magma transport and petroleum systems within sedimentary basins. Basin Res. https://doi.org/10.1111/bre.12164.
Schofield, N., Stevenson, C.T., Reston, T., 2010. Magma fingers and host rock fluidization in the emplacement of sills. Geology 38, 63–66. https://doi.org/10.1130/g30142.1.
Senger, K., Buckley, S.J., Chevallier, L., Fagereng, Å., Galland, O., Kurz, T., Ogata, K., Planke, S., Tveranger, J., 2015. Fracturing of doleritic intrusions and associated contact zones: insights from the Eastern Cape, South Africa. J. Afr. Earth Sci. 102, 70–85.
Senger, K., Millett, J., Planke, S., Ogata, K., Eide, C.H., Festøy, M., Galland, O., Jerram, D.A., 2017. Effects of igneous intrusions on the petroleum system: a review. First Break 35, 47–56. https://doi.org/10.3997/1365-2397.2017011.
Sernageomin, 2003. Mapa Geológico de Chile: versión digital.
Silvestro, J., Atencio, M., 2009. La cuenca cenozoica del río Grande y Palauco: edad, evolución y control estructural, faja plegada de Malargüe. Rev. Asoc. Geol. Argent. 65, 154–169.
Silvestro, J., Kraemer, P., 2005. Evolución Tectosedimentaria de la Cordillera Principal en el sector Surmendocino a los 35 30'S. Faja plegada de Malargue, República Argentina.

In: Congreso de exploración y desarrollo de hidrocarburos.
Smith, R.P., 1987. Dyke emplacement at Spanish peaks, Colorado. In: Halls, H.C., Fahrig, W.F. (Eds.), Mafic Dike Swarms. Geological Association of Canada Special Paper, pp. 47–54.
Søager, N., Holm, P.M., Llambías, E.J., 2013. Payenia volcanic province, southern Mendoza, Argentina: OIB mantle upwelling in a backarc environment. Chem. Geol. 349–350, 36–53. https://doi.org/10.1016/j.chemgeo.2013.04.007.
Spacapan, J.B., D'Odorico, A., Palma, O., Galland, O., Senger, K., Ruiz, R., Manceda, R., Leanza, H.A., 2019. Low resistivity zones at contacts of igneous intrusions emplaced in organic-rich formations and their implications on fluid flow and petroleum systems: a case study in the northern Neuquén Basin, Argentina. Basin Res. 0. https://doi.org/10.1111/bre.12363.
Spacapan, J.B., Galland, O., Leanza, H.A., Planke, S., 2017. Igneous sill and finger emplacement mechanism in shale-dominated formations: a field study at Cuesta del Chihuido, Neuquén Basin, Argentina. J. Geol. Soc. 174, 422–433. https://doi.org/10.1144/jgs2016-056.
Spacapan, J.B., Palma, O., Galland, O., Manceda, R., Rocha, E., D'Odorico, A., Leanza, H.A., 2018. Thermal impact of igneous sill complexes on organic-rich formations and the generation of a petroleum system: case study in the Neuquén Basin, Argentina. Mar. Petrol. Geol. 91, 519–531. https://doi.org/10.1016/j.marpetgeo.2018.01.018.
Svensen, H., Planke, S., Chevallier, L., Malthe-Sorenssen, A., Corfu, F., Jamtveit, B., 2007. Hydrothermal venting of greenhouse gases triggering Early Jurassic global warming. Earth Planet. Sci. Lett. 256, 554–566.
Svensen, H., Planke, S., Malthe-Sorenssen, A., Jamtvelt, B., Myklebust, R., Eldem, T.R., Rey, S.S., 2004. Release of methane from a volcanic basin as a mechanism for initial Eocene global warming. Nature 429, 542–545.
Symonds, P.A., Planke, S., Frey, O., Skogseid, J., 1998. Volcanic evolution of the Western Australian continental margin and its implications for basin development. In: Purcell, P.G., Purcell, R.R. (Eds.), The Sedimentary Basins of Western Australia: Proceedings of the Petroleum Exploration Society of Australia Symposium. Petroleum Exploration Society of Australia, Perth, pp. 33–54.
Thomson, K., 2004. Volcanic features of the North Rockall Trough: application of visualisation techniques on 3D seismic reflection data. Bull. Volcanol. 67, 116–128.
Thomson, K., 2007. Determining magma flow in sills, dykes and laccoliths and their implications for sill emplacement mechanisms. Bull. Volcanol. 70, 183–201.
Thomson, K., Hutton, D., 2004. Geometry and growth of sill complexes: insights using 3D seismic from the North Rockall Trough. Bull. Volcanol. 66, 364–375.
Thorey, C., Michaut, C., 2016. Elastic-plated gravity currents with a temperature-dependent viscosity. J. Fluid Mech. 805, 88–117. https://doi.org/10.1017/jfm.2016.538.
Trude, J., Cartwright, J., Davies, R.J., Smallwood, J., 2003. New technique for dating igneous sills. Geology 31, 813–816.
Tunik, M., Folguera, A., Naipauer, M., Pimentel, M., Ramos, V.A., 2010. Early uplift and orogenic deformation in the Neuquén Basin: constraints on the Andean uplift from U–Pb and Hf isotopic data of detrital zircons. Tectonophysics 489, 258–273.
Vergani, G.D., Tankard, A.J., Belotti, H.J., Welsink, H.J., 1995. Tectonic Evolution and Paleogeography of the Neuquén Basin, Argentina.
Walker, G.P.L., 1975. Intrusive sheet swarms and the identity of Crustal Layer 3 in Iceland. J. Geol. Soc. Lond. 131, 143–159. https://doi.org/10.1144/gsjgs.131.2.0143.
Westerman, D.S., Rocchi, S., Breitkreuz, C., Stevenson, C.T., Wilson, P.I.R., 2018. Structures related to the emplacement of shallow-level intrusions. In: Breitkreuz, C., Rocchi, S. (Eds.), Physical Geology of Shallow Magmatic Systems: Dykes, Sills and Laccoliths. Springer International Publishing, Cham, pp. 83–118.
White, R.S., Drew, J., Martens, H.R., Key, J., Soosalu, H., Jakobsdóttir, S.S., 2011. Dynamics of dyke intrusion in the mid-crust of Iceland. Earth Planet. Sci. Lett. 304, 300–312. https://doi.org/10.1016/j.epsl.2011.02.038.
Wilson, P.I.R., McCaffrey, K.J.W., Wilson, R.W., Jarvis, I., Holdsworth, R.E., 2016. Deformation structures associated with the Trachyte Mesa intrusion, Henry Mountains, Utah: implications for sill and laccolith emplacement mechanisms. J. Struct. Geol. 87, 30–46. https://doi.org/10.1016/j.jsg.2016.04.001.
Witte, J., Bonora, M., Carbone, C., Oncken, O., 2012. Fracture evolution in oil-producing sills of the Rio Grande Valley, northern Neuquén Basin, Argentina. AAPG Bull. 96, 1253–1277. https://doi.org/10.1306/10181110152.